

ANALYZING RECEPTOR RESPONSES IN THE *DROSOPHILA*  
JOHNSTON'S ORGAN WITH TWO-PHOTON MICROSCOPY

DISSERTATION FOR THE AWARD OF THE DEGREE  
"DOCTOR RERUM NATURALIUM"  
OF THE GEORG-AUGUST-UNIVERSITÄT GÖTTINGEN

WITHIN THE DOCTORAL PROGRAM "SENSORY AND MOTOR NEUROSCIENCE"  
OF THE GEORG-AUGUST UNIVERSITY SCHOOL OF SCIENCE (GAUSS)

SUBMITTED BY PHILIPP JÄHDE  
FROM HESSISCH-LICHTENAU  
GÖTTINGEN, 2016

## THESIS COMMITTEE

Prof. Dr. Martin Göpfert  
Department of cellular neurobiology,  
University of Göttingen

Prof. Dr. André Fiala  
Department of molecular neurobiology of behaviour,  
University of Göttingen

Prof. Dr. Siegrid Löwel  
Department of systems neuroscience,  
University of Göttingen

## MEMBERS OF THE EXAMINATION BOARD

Referee: Prof. Dr. Martin Göpfert  
Department of cellular neurobiology,  
University of Göttingen

2<sup>nd</sup> Referee: Prof. Dr. André Fiala  
Department of molecular neurobiology of behaviour,  
University of Göttingen

## FURTHER MEMBERS OF THE EXAMINATION BOARD

Prof. Dr. Siegrid Löwel  
Department of systems neuroscience,  
University of Göttingen

Dr. Manuela Schmidt  
Somatosensory signaling group,  
Max Planck Institute of Experimental Medicine

Dr. Marion Silies  
Visual processing group,  
European Neuroscience Institute Göttingen

Prof. Dr. Tobias Moser  
Inner ear lab,  
University Medical Center Göttingen

Date of oral examination: August 24<sup>th</sup>, 2016

## DECLARATION

---

Herewith I declare that I prepared this doctoral thesis entitled “Analyzing receptor responses in the *Drosophila* Johnston’s organ with two-photon microscopy” on my own, with no other sources and aids than quoted.

Göttingen, June 9<sup>th</sup>, 2016

---

Philipp Jähde



## ABSTRACT

---

Hearing organs rely on force-gated ion channels to convert the mechanical energy imposed by sound into receptor potentials usable by the nervous system. So far, little is known about the identity and working mechanisms of these channels, but in recent years several candidate proteins have emerged which seem to be key elements of force transduction systems.

In the fruit fly *Drosophila melanogaster*, two proteins involved in the function of several mechanosensory organs are the transient receptor potential channel subunits Inactive and NompC (No mechanoreceptor potential C). Mutations of both proteins strongly impair the function of many mechanosensory organs, an influence which has been best studied in the Johnston's organ (JO), the mechanosensitive neurons of the *Drosophila* ear.

Recent studies came to different conclusions about the specific roles of Inactive and NompC, but all of them agree in the observations that loss of Inactive changes the active amplification properties of the JO, and disrupts the transmission of auditory signals into the brain. Mutations of NompC instead prevent active amplification of faint sounds, but the JO retains a certain amount of sound sensitivity.

All of these studies used experimental methods lacking spatial resolution, and thus had to base their conclusions on the response of large groups of JO neurons. In this thesis I adopted an existing widefield calcium imaging method for two-photon excitation microscopy, increasing the spatial resolution to single scolopidia (assemblies of two to three sensory neurons). This method thus allowed me to study the influence of *nompC*- and *inactive* mutations on individual receptor units of the JO.

Measuring individual responses of the JO neurons of control flies revealed a much higher diversity of response characteristics as distinguishable before. While the separation into highly sound-sensitive and less sensitive wind-detecting neurons found in earlier studies could in general be confirmed, especially the more sensitive cells showed a much larger response variability than detectable with group recording methods.

Analysis of sound responses in mutant backgrounds revealed that both mutations do not remove the mechanosensitivity of all sensory neurons: Whereas *inactive* leaves small residual responses in some sensory neurons, *nompC* leads to several different response changes. Differing from earlier studies, some of the sound-sensitive cells remain mechanosensitive (even though with decreased sensitivity) and only in a few sound responses are abolished. In addition, several JO neurons react to sound stimulation with a negative calcium signal, which is a so far unobserved effect of the *nompC* mutation.

Concluding from my results, neither Inactive nor NompC are "the" transduction channel of all *Drosophila* auditory neurons. Which roles they play in mutant neurons with remnant mechanosensitivity remains to be investigated.



## CONTENTS

---

1	INTRODUCTION	1
1.1	The hearing organ of <i>Drosophila melanogaster</i>	2
1.2	Johnston's organ	3
1.2.1	Subdivision of the Johnston's organ	4
1.2.2	Mechanotransduction in the Johnston's organ	4
1.3	Nanchung and Inactive	5
1.4	NompC	5
1.5	Role of Inactive and NompC in the Johnston's organ	6
1.6	Aim and experimental approach	7
2	MATERIALS AND METHODS	11
2.1	Imaging setup	11
2.2	Preparation	12
2.3	Stimulation	12
2.4	Data analysis	14
2.4.1	Image processing	14
2.4.2	Fits and cluster analysis	15
2.5	Flies	15
2.6	Scanning electron microscopy	17
3	RESULTS	19
3.1	Comparison between single-photon excitation widefield imaging and two-photon scanning microscopy data	19
3.2	Response of receptor units to arista deflection	19
3.2.1	Sinusoidal stimulation	19
3.2.2	Mixed stimulation	21
3.3	Signal dynamics within receptor units	21
3.4	Intensity-response curves	25
3.4.1	Differences to electrophysiology data	25
3.4.2	Receptor unit subgroups	25
3.4.3	Response of subgroup A/B-neurons	26
3.5	<i>inactive</i> mutants	32
3.5.1	Dendritic signals in <i>inactive</i> mutants	32
3.5.2	Cell body- and axonal signals in <i>inactive</i> mutants	34
3.6	<i>nompC</i> mutants	34
3.6.1	Response of all JO neurons in <i>nompC</i> mutants	35
3.6.2	Response of A/B neurons in <i>nompC</i> mutants	35
4	DISCUSSION	41
4.1	Two-photon calcium imaging in the Johnston's organ	41
4.2	Single receptor unit responses	42
4.2.1	Fits and cluster analysis	42
4.3	Influence of the <i>inactive</i> mutation	43
4.4	Influence of the <i>nompC</i> mutation	45
4.4.1	<i>nompC<sup>3</sup></i> , all JO neurons	45
4.4.2	<i>nompC<sup>3</sup>/nompC<sup>1</sup></i> , A/B neurons	46

4.5 Outlook 47

BIBLIOGRAPHY 49

ACKNOWLEDGEMENTS 57

CURRICULUM VITAE 59



## LIST OF FIGURES

---

Figure 1.1	Electron micrograph of the antenna / 2p scan of the pedicel	2
Figure 1.2	Horizontal section of the jo	3
Figure 1.3	Drawing of a single scolopidium	3
Figure 1.4	NompC as primary transduction channel	7
Figure 1.5	Inactive as primary transduction channel	8
Figure 1.6	Comparison between 1p- and 2p-imaging	9
Figure 2.1	Fly holder	13
Figure 2.2	Tip displacement extrapolation	14
Figure 3.1	Comparison between 2p and epifluorescence raw data	20
Figure 3.2	Sensitivity differences between individual receptor units	21
Figure 3.3	JO response to additional sustained deflection	22
Figure 3.4	Signal dynamics within single receptor units	24
Figure 3.5	Cluster analysis of all JO neurons	27
Figure 3.6	Cluster analysis of all JO neurons, whitened	28
Figure 3.7	Labeling of A/B neurons via 6XmCherry	29
Figure 3.8	Cluster analysis of A/B-neurons	30
Figure 3.9	Cluster analysis of A/B-neurons, whitened	31
Figure 3.10	Dendritic signals in <i>inactive</i> mutants	33
Figure 3.11	Axonal, cell body and dendritic signals in <i>inactive</i> mutants	34
Figure 3.12	Cluster analysis of <i>nompC<sup>3</sup>/nompC<sup>3</sup></i> flies	36
Figure 3.13	Cluster analysis of <i>nompC<sup>3</sup>/nompC<sup>3</sup></i> flies, whitened	37
Figure 3.14	Calcium signals in A/B cells of <i>nompC<sup>3</sup>/nompC<sup>1</sup></i> flies, I	39
Figure 3.15	Calcium signals in A/B cells of <i>nompC<sup>3</sup>/nompC<sup>1</sup></i> flies, II	40
Figure 4.1	Influence of Inactive on membrane potential propagation	44

## LIST OF TABLES

---

Table 3.1	Single receptor unit fit results	23
-----------	----------------------------------	----

## ACRONYMS

---

JO	Johnston's Organ
GFN	Giant Fibre Neuron
TRP	Transient Receptor Potential
ROI	Region of Interest
GEVI	Genetically Encoded Voltage Indicator
GECI	Genetically Encoded Calcium Indicator
AIC	Akaike Information Criterion

## INTRODUCTION

---

We rely on our senses to survive in an environment where we constantly have to react to the influence of a multitude of highly dynamic external stimuli. The basis of this complex interaction are our sensory organs, which perform the detection of environmental influence such as electromagnetic waves, mechanical force, temperature, or chemicals, but also serve as first filters, restricting the spectrum of perceivable information to a range that is necessary for us to survive. While some sensory organs rival our most precise measuring instruments, others rather report a coarse approximation of a stimulus. Nevertheless, all sensory organs rely on the same basic principle: The conversion of various forms of energy into information usable by the organism. Whereas some of these conversion processes are believed to be quite well understood, others remain rather obscure.

One of the lesser understood systems is the detection of mechanical stimuli, which is one of the most widespread and important abilities of living things. Even unicellular organisms without specialized sensory cells are capable of reacting to mechanical influence such as membrane- and cytoskeleton stretch induced by noxious osmotic environments, surface adhesion or fluid flow (Blount et al., 1999; Booth et al., 2007; Zhu et al., 2015). In higher organisms, mechanosensation provides the functional basis of touch, proprioception, nociception and hearing, allowing dexterous manipulation of objects, coordinated movement, acoustic communication and a multitude of other sophisticated behavioral tasks (Akitake et al., 2015; Dubin et al., 2010; Fettiplace et al., 2014; Maksimovic et al., 2014).

The corresponding sensory organs utilize a variety of macroscopic functional principles to measure the force induced by a stimulus, yet the underlying sensory cells share strong functional and genetic similarities on a microscopic level even in distantly related organisms. This similarity of basic functional principles makes the use of model organisms an interesting option to study the transduction of mechanical stimuli in systems where powerful experimental tools are available, even though the sensory organs as a whole differ a lot.

This macroscopic difference is quite distinct between the tympanal hearing organs of most vertebrates and the flagellar ears of the fruit fly *Drosophila melanogaster*. Still, genetic screens report a surprising number of genes involved in both systems, ranging from developmental genes to motor proteins and ion channels (Ben-Arie et al., 2000; Senthilan et al., 2012). Furthermore, studies of the sensory cells' mechanical properties reveal striking similarities, such as the use of active amplification of mechanical stimuli to boost the ear's sensitivity in both systems (Göpfert et al., 2006; Hudspeth, 2008). Therefore, *Drosophila melanogaster* with its one century of genetic research history, little ethical problems, easy breeding and lower costs compared to

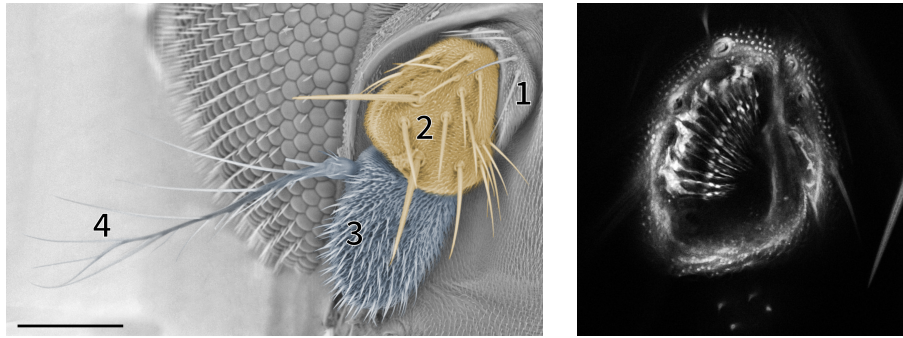


Figure 1.1: LEFT: ANTERIOR VIEW OF *DROSOPHILA MELANOGASTER*'S ANTENNA The antenna of *Drosophila* is divided into three segments: The scape (1), the pedicel (2, light brown) and the funiculus (3, blue). The funiculus is covered with chemosensory sensilla and has a feather-like appendage, the arista (4), which acts as a contact surface for sound particle movement. The pedicel encloses the sensory neurons of the Johnston's organ (JO) and is connected to the funiculus via a twistable joint. The scape contains muscles which can move pedicel and funiculus. Scalebar=100  $\mu\text{m}$  RIGHT: TWO-PHOTON IMAGE OF THE PEDICEL A maximum projection of five two-photon excitation images of the pedicel shows the circular arrangement of the JO neurons, visualized by expression of GCaMP.

research on mammals is a worthwhile subject to investigate the molecular basis of mechanosensation.

### 1.1 THE HEARING ORGAN OF *DROSOPHILA MELANOGASTER*

Like the ears of vertebrates, the hearing organ of *Drosophila melanogaster* detects perturbations of its surrounding medium and converts them into neuronal signals usable by the nervous system (Ewing, 1978; Göpfert et al., 2002). In the case of adult *Drosophila*, the carrier medium is air and the main behavioural use of hearing is intraspecific communication, like the perception of the male courtship song and sound signals created during agonistic interactions of males (Jonsson et al., 2011; Schilcher, 1976).

The hearing organ of *Drosophila* is a flagellar ear and thus uses a very different mechanism to detect sound than the tympanal ears of vertebrates. Instead of measuring air pressure or pressure gradient changes via a tympanum, it detects the particle velocity component of sound via a very light, movable part of its antenna (Bennet-Clark, 1971).

This sound receiver is formed by the second and third segment of its antenna, which features a feather shaped appendage, the arista (Fig. 1.1, 4). It acts as a contact surface for sound particles and is rigidly connected to the third antennal segment, the funiculus. The funiculus, in turn, is connected to the second antennal segment (the pedicel) via a movable joint (Bennet-Clark, 1971; Manning, 1967). Therefore, the sound-induced displacement of the arista is converted to a rotational motion of the funiculus, which translates to a deformation of the cuticle at the joint to the pedicel (Fig. 1.2). This deformation is then detected by the sensory neurons of the Johnston's Organ (JO) (Eberl et al., 2000; Göpfert et al., 2002), which is *Drosophila*'s largest

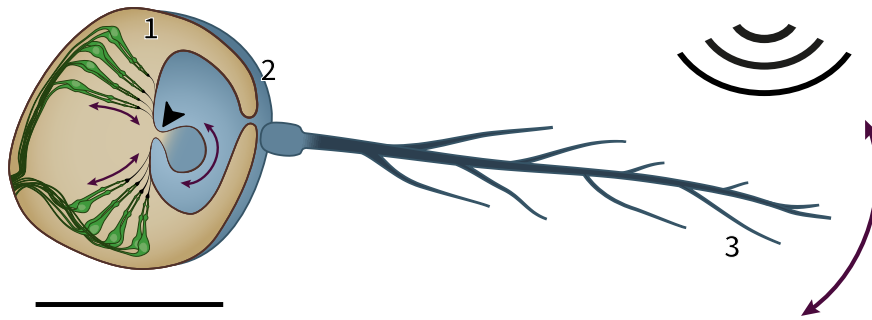


Figure 1.2: HORIZONTAL SECTION THROUGH THE JO The neurons of the JO are connected to the movable joint (arrowhead) between pedicel (1) and funiculus (2). Motion of the arista (3) therefore leads to stretch and compression of the sensory neurons. Because of the long lever formed by the arista, the resulting displacements at the sensory neurons reach down to the sub-nm range. Scalebar: 100 $\mu$ m

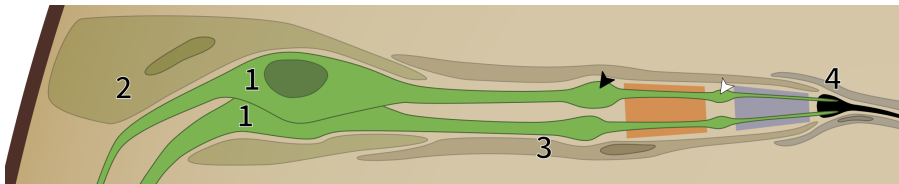


Figure 1.3: THE SCOLOPIDIUM The scolopidia are the receptor units of Johnston's organ and consist of two to three sensory neurons (1) and three support cells. The ligament cell (2) anchors the base of the sensory neurons to the wall of the pedicel. A scolopale cell (3) surrounds the neuron's dendrites and forms the scolopale space around them, an endolymph environment believed to be  $K^+$ -rich (in analogy to bristles and campaniform sensilla, Todi et al., 2004). The tip of the scolopidium is connected to the antennal joint via the dendritic cap and cap cells (4), which in katydids also contribute to the ion composition of the receptor endolymph (Oldfield et al., 1986) Orange area: expression site of Inactive, blue area: expression site of NompC. Black arrow: basal body, white arrows: ciliary dilation.

chordotonal organ and was named after Christopher Johnston, who first described a similar assembly of cells in the mosquito *Culex pipiens* as a putative hearing organ (Johnston, 1855).

## 1.2 JOHNSTON'S ORGAN

The ca. 480 bipolar neurons of the JO are organized in sensory units called scolopidia, which are formed by two or three sensory neurons and three support cells (Fig.1.3, Shigekazu et al. 1965; Todi et al. 2004). The support cells are wrapped around the sensory neurons and control the receptor lymph environment between them, in addition to anchoring them to the surrounding tissue (Roy et al., 2013), with the tips of the scolopidia converging towards the antennal joint between second and third antennal segment.

The physiology of the JO has been studied with several different experimental methods, including compound action potential recordings from the antennal nerve, whole-cell voltage clamp recordings of neurons receiving in-

put from the JO, widefield-calcium imaging of the whole hearing organ, and Laser Doppler Vibrometry (Eberl et al., 2000; Göpfert et al., 2002; Kamikouchi et al., 2009; Lehnert et al., 2013; Tootoonian et al., 2012).

These studies revealed a striking similarity to the vertebrate ear: Just like vertebrate hair cells, the JO neurons not only detect sound-induced motion, but also create motion themselves (Davis, 1983; Fettiplace, 2006). By phase-locking this motion to the displacement of the arista, the JO neurons amplify faint sounds, thus increasing the sensitivity of the hearing organ in the behaviourally most relevant frequency spectrum (Göpfert et al., 2005, 2003).

### 1.2.1 *Subdivision of the Johnston's organ*

Further investigation of these properties showed that not all neurons of the JO contribute equally to the active amplification of sound, but are rather subdivided into groups with different stimulus preferences (Kamikouchi et al., 2009; Yorozu et al., 2009). The subdivision of the JO neurons was first suspected from the cluster-forming anatomy of their axon terminals in the brain, which Kamikouchi et al., 2006 used to classify the JO neurons into the five subgroups A–E. Functional analysis of these subgroups showed that subgroups A, B and D react mainly to vibrational stimuli with high sensitivity, whereas C and E prefer sustained deflection as caused by gravity and wind (Kamikouchi et al., 2009; Matsuo et al., 2014; Yorozu et al., 2009). Furthermore, active amplification of faint sounds is lost when the sound-sensitive subgroups A and B are ablated, but remains when the C/E neurons are silenced (Effertz et al., 2011).

### 1.2.2 *Mechanotransduction in the Johnston's organ*

Modeling of the JO's active properties implies that a transduction complex consisting of a gating spring and motor- and channel proteins alone could provide the force needed for amplification, but the specific members of this complex are still unclear (Nadrowski et al., 2008). Since electrophysiological recordings show very fast responses of the JO neurons to mechanical stimuli, it is assumed that at least one directly force-gated ion channel is involved in the transduction mechanism of the cells (Albert et al., 2007; Lehnert et al., 2013). This assumption is further supported by measurements of the mechanical properties of the antennal sound receiver, where traces of actual channel gating can be observed as a fast response to step displacements of the arista (Albert et al., 2007), similar to the gating compliances measured in bullfrog haircells (Howard et al., 1988).

There are several proteins known to be involved in this transduction machinery, amongst them motor proteins, ion channels and scaffolding proteins, yet their specific roles are still under debate (Effertz et al., 2011; Gong et al., 2004; Karak et al., 2015; Senthilan et al., 2012).

Three promising candidates for the mechanosensory channel of the JO neurons are the Transient Receptor Potential (TRP) channel subunits Inactive, Nanchung and NompC. All of them are expressed in distal parts of the JO

neuron's dendrites and are required for proper amplification and transduction of mechanical stimuli (Effertz et al., 2012; Gong et al., 2004; Kim et al., 2003; Lee et al., 2010; Lehnert et al., 2013).

### 1.3 NANCHUNG AND INACTIVE

Inactive and Nanchung are the only two members of the TRP vanilloid channel subfamily in *Drosophila* and are both necessary for the proper function of several types of mechanosensors, including the neurons of the JO. Inactive was first described in a behavioral screen as *hypoB*, where mutant flies showed reduced locomotor activity (Homyk, 1977), whereas Nanchung was predicted to be a TRPV channel from its DNA sequence (Kim et al., 2003). Together they seem to form a heteromultimeric cation channel (Nesterov et al., 2015), which in the JO neurons localizes to the distal part of the dendrites, between basal body and ciliary dilation (Fig 1.3; Gong et al., 2004).

Mutations of either Inactive or Nanchung lead to a loss of sound-evoked local field potentials at the antennal nerve, reduced motor activity, impaired gravitaxis and strong spontaneous oscillations of the sound receiver at a lower frequency than wildtype flies (Gong et al., 2004; Göpfert et al., 2006; Kim et al., 2003; Sun et al., 2009). There are contradicting results whether Inactive and Nanchung are mechanosensitive, as Nesterov et al., 2015 could not reproduce the activation by hypoosmotic stress in heterologous expression as performed by Gong et al., 2004 and Kim et al., 2003.

Nonlinear amplification of the arista motion is still present in *inactive* and *nanchung* mutants, though with an eightfold increase in gain (Göpfert et al., 2006). Since phase locked amplification of sound inherently requires to sense the sound induced motion, some form of mechanotransduction still has to be present in these mutants. In addition, Kamikouchi et al., 2009 and Wiek, 2013 observed remaining calcium influx into JO neurons in *nanchung* and *inactive* mutants. Therefore, these results point to a role of Inactive and Nanchung in the modulation of active amplification and to the existence of at least one more mechanosensitive element in the JO neurons.

As no receptor potentials are measurable anymore at the antennal nerve and the gap-junction-coupled Giant Fibre Neuron (GFN) (Kim et al., 2003; Lehnert et al., 2013), Inactive and Nanchung might also be involved in the propagation of the transduction current along the dendrite of the sensory neurons. In this case, the actual transduction event could still happen, yet no dendritic signal would reach the cell bodies and axons, leading to the observed absence of local field potentials at the antennal nerve and lack of voltage clamp signals at the GFN.

### 1.4 NOMPC

The *nompC* mutation was first discovered in a screen for mechanosensation-related genes based on leg coordination of adult flies (Kernan et al., 1994). Besides leading to severe uncoordination, *nompC*-null mutations showed almost completely abolished transduction currents in mechanosensitive thorax

bristles, highlighting NompC as an important part of their transduction machinery (Walker, 2000). Several other studies found NompC to be vital for a multitude of processes relying on mechanotransduction, such as the perception of gentle touch in larvae, hearing in adults and leg posture control. In these processes it is necessary for the function of ciliated as well as multidendritic sensory neurons (Chadha et al., 2015; Effertz et al., 2011; Yan et al., 2013).

Mutations of NompC homologs in other species also lead to malfunction of mechanosensory cells: An ortholog of NompC was shown to be essential for electrical responses in hair cells of zebrafish larvae (Sidi et al., 2003), whereas another one in *C. elegans*, TRP-4, is required in sensory cilia (Kang et al., 2010).

In addition to expression in mechanosensory neurons and being crucial for their proper response, NompC shows further necessary properties of a mechanosensitive channel (Arnadóttir et al., 2010): Point mutations change the transduction currents (Gong et al., 2013; Kang et al., 2010; Walker, 2000) and heterologous as well as ectopic expression makes non-mechanosensitive cells sensitive to mechanical stimulation (Gong et al., 2013; Yan et al., 2013).

An additional interesting feature of NompC are the 29 cytosolic ankyrin repeats at its N terminus. They form one helical spring-shaped turn and tether the channel to the dendrite's axoneme (Liang et al., 2013; Zhang et al., 2015), which could enable the channel to sense cell membrane motion relative to the cytoskeleton. Fusing these ankyrin repeats to a voltage-gated, mechanoinensitive potassium channel (Kv2.1) resulted in a mechanical force-gated chimeric channel (Zhang et al., 2013).

### 1.5 ROLE OF INACTIVE AND NOMPC IN THE JOHNSTON'S ORGAN

Even though these studies offer strong evidence that NompC is indeed a mechanosensitive channel or channel subunit, its role in the Johnston's organ is still under debate. In *nompC* null mutants acoustic stimuli still elicit local field potentials in the antennal nerve, indicating that mechanotransduction in the hearing organ is not completely lost in the absence of NompC (Eberl et al., 2000). Closer analysis of NompC's influence on subunits of the JO via calcium imaging (Effertz et al., 2011) suggests it is only necessary for mechanotransduction in the sound-sensitive group A and B neurons, making a different, unknown channel responsible for the remaining field potentials and calcium signals in *nompC* mutants. These results are supported by the changed mechanical properties of the sound receiver in *nompC* mutants, as the reduction of the gating compliance resembles the phenotype of flies with ablated sound-sensitive neurons (Effertz et al., 2012).

Voltage clamp recordings from the GFN though detected sound-evoked currents in *nompC* mutants (Lehnert et al., 2013), which would contradict the calcium imaging data from Effertz et al., since based on the overlap of their projections, only the sound-sensitive A/B neurons seem to form electrical synapses with the GFN (Kamikouchi et al., 2006; Lehnert et al., 2013). As the sound-evoked GFN currents in *nompC* mutants are only elicited at high stimulus intensities, Lehnert et al. conclude that NompC is only responsible for



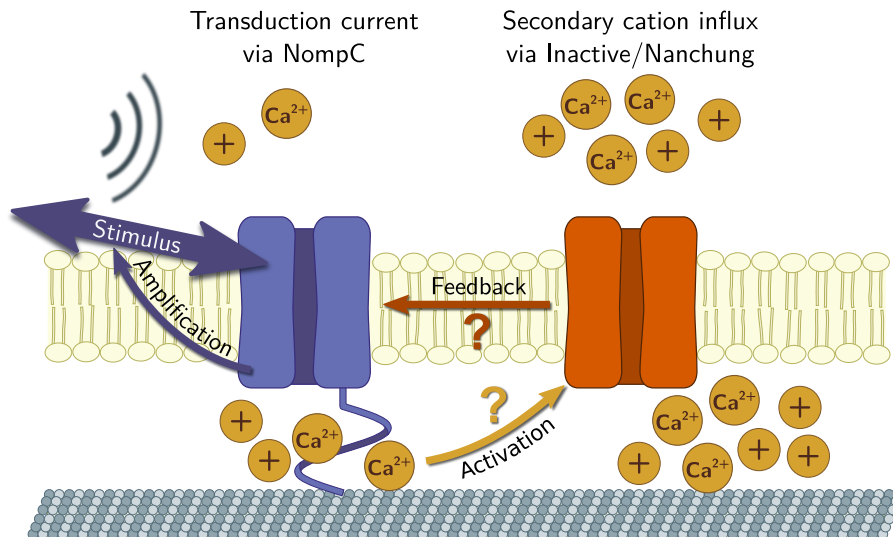


Figure 1.4: **NOMPC AS PRIMARY TRANSDUCTION CHANNEL** According to the studies of Effertz et al., 2012 and Göpfert et al., 2006, NompC might be the mechanosensitive channel of the sound-sensitive JO neurons, whereas Inactive modulates the feedback amplification promoted by NompC. Opening of Inactive via a currently unknown process could then lead to an additional cation influx into the neuron, leading to a boost of the electrical signal propagating along the dendrite.

the mechanical feedback amplification of the JO and that the actual transduction is performed by Inactive. However, Mu et al., 2014 suggest that also neurons of the wind-sensitive JO group E form connections with the GFN, which could give rise to the NompC-independent transduction currents at sufficiently high sound intensities. This could bring the data of Lehnert et al. in accordance with the results of Effertz et al., even though their initial conclusions regarding the function of NompC in the JO were contradicting.

## 1.6 AIM AND EXPERIMENTAL APPROACH

It is possible that the discrepancies in the interpretation of the currently available studies regarding the roles of NompC and Inactive are to some extent due to a general drawback of the employed methods: All of them record summed responses of large JO neuron groups at once, thereby masking effects mutations might have on smaller subgroups. In the case of the first antennal nerve recordings in *nompC* mutants (Eberl et al., 2000), the resulting reduced signal amplitudes could either be interpreted as a slightly impaired transduction in all neurons, or an entire loss in some of them, leading to very different interpretations of NompC's role in these cells.

Whole-cell voltage clamp recordings of single sensory neurons would of course yield valuable data about the transduction currents in the JO, but are probably impossible to perform: Since the cuticle of the antenna is an integral part of the *Drosophila* ear, penetrating the pedicel with electrodes alters its response properties, thus compromising the recorded data. Furthermore, damaging the support cells wrapped around the sensory neurons would most

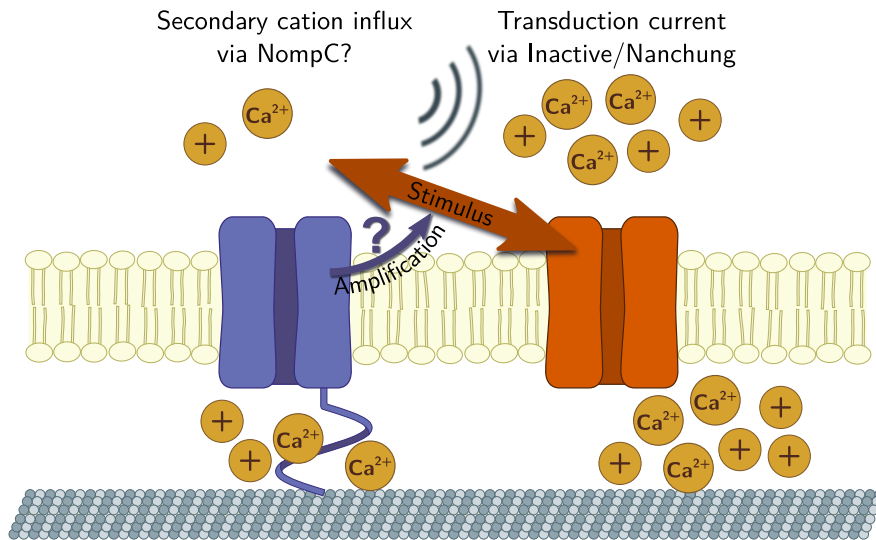
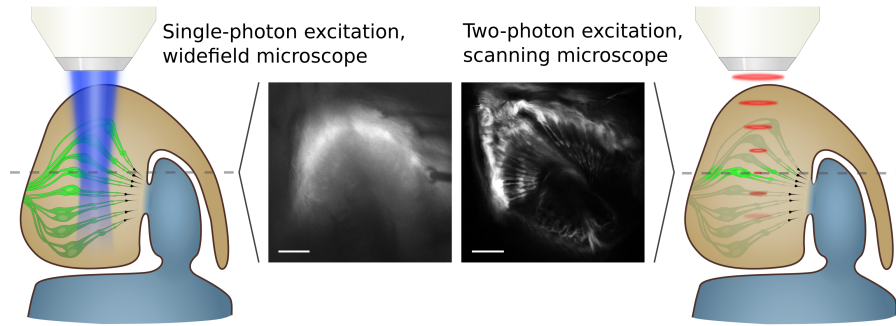


Figure 1.5: INACTIVE AS PRIMARY TRANSDUCTION CHANNEL According to the study of Lehnert et al., 2013, Inactive might be the primary mechanosensitive channel of the sound-sensitive JO neurons, whereas NompC only promotes the active feedback amplification of the mechanical stimulus gating Inactive.

likely render the whole scolopidium dysfunctional. Thus, all current studies used methods which are non-invasive (at least at the antenna) to probe the function of the JO neurons, at the cost of losing information about the precise origin of the measured signals.

In this study, I will try to further clarify the roles of NompC and Inactive by investigating their influence on the response of individual JO receptor units. To improve upon the bulk-recording limit of the previous studies, I am using two-photon excitation calcium imaging (Denk et al., 1990). Due to its optical sectioning, I will be able to monitor the activity of many sensory neurons simultaneously, avoiding the crosstalk from out-of-focus cells present with single-photon excitation (Fig 1.4). The optical resolution of the two-photon microscope should be sufficient to tell apart individual receptor units of the JO and therefore also allow to observe potential differences in their reaction to the *nompC* and *inactive* mutations.

Furthermore, since the spatial resolution should be sufficient to observe calcium signal differences within receptor units, it might be possible to unravel whether the *inactive* mutation merely disrupts the signal propagation along the dendrites, or if it leads to a complete loss of cation influx into the cells.



**Figure 1.6: COMPARISON BETWEEN SINGLE- AND TWO-PHOTON EXCITATION**  
 In single photon excitation fluorescence microscopy, fluorophores absorb one photon of the excitation light and emit a photon with longer wavelength. In the case of GCaMP6m, the most efficient excitation wavelength is around 480 nm, whereas emission is usually detected in the range between 500 and 550 nm. As GCaMP fluorescence happens in the whole volume covered by the excitation light, emitted light is also collected from below and above the focal plane, essentially leading to a summation of the signals of all illuminated JO neurons in the camera image. The response of individual receptor units can therefore not be separated and potential response variability becomes averaged. In addition, also photobleaching is happening in the whole organ at once. Two-photon excitation microscopy utilizes the effect that also two long-wavelength photons (~950 nm for GCaMP6) can provide the necessary energy to excite a fluorophore when they reach the molecule temporally close enough. Since the two photons have to arrive in a time range of one attosecond, high photon densities are necessary at the fluorophore to increase the probability of a two-photon absorption event. To achieve a sufficient photon flux, mode-locked femtosecond lasers are used, which compress light into short (~120 fs), high-energy pulses. The additional spatial compression of the excitation light in the focal volume of the microscope objective then increases the photon density enough to enable two-photon absorption. Above and below the focal plane the unfocused laser pulses do not provide sufficient photon flux to facilitate two-photon excitation, thus creating neither out-of-focus fluorescence nor photobleaching. Therefore, the resulting image resembles an optical section through the sample at the focal plane, which allows the spatial localization of calcium sensor signals from individual JO receptor units even in volumes where they would be concealed with single photon excitation. Scalebar: 20  $\mu\text{m}$ , color of antenna segments as in Fig.1.1



## MATERIALS AND METHODS

---

To reach single-cell resolution of the JO's response to sound- and wind-like stimuli, a two-photon calcium imaging setup was established. Besides being non-invasive, two-photon imaging has the advantage of providing information about the spatial origin of the signals and therefore allows to simultaneously monitor multiple neurons. In the following, the equipment and procedures used in the two-photon imaging experiments are described.

### 2.1 IMAGING SETUP

Two-photon excitation calcium imaging was performed with an imaging setup consisting of a Zeiss LSM 7 MP scanning microscope (Carl Zeiss, Jena) coupled with a Chameleon Vision II titanium sapphire laser (Coherent Inc., Santa Clara) as multiphoton excitation light source. ZEN 2011 was used as image acquisition and microscope/laser control software.

The Genetically Encoded Calcium Indicator (GECI) GCaMP6m (Chen et al., 2013) was used to measure the activity of the JO neurons. GCaMP is a fusion protein consisting of a circularly permuted GFP, a calmodulin and the M13 fragment of a myosin light chain kinase (Nakai et al., 2001). Binding of calcium to the calmodulin domain leads to a conformation change of the protein which greatly increases its fluorescence. The current GCaMP6 family reaches signal-to-noise ratios similar to synthetic calcium sensors, but has the advantage of being expressible in specific cell types via the GAL4/UAS and LexA/LexAOp systems (Brand et al., 1993; Lai et al., 2006). A GAL4 line specific for the sound-sensitive subgroups A and B (Kamikouchi et al., 2006; Sharma et al., 2002) was used to drive UAS-6XmCherry (Shearin et al., 2014) reporter expression, and nSyb-LexA (Shearin et al., 2013) was used to drive LexAOp-GCaMP6m. This allowed to assign neurons to the sound-sensitive subgroups based on mCherry-expression, although all JO neurons expressed GCaMP6m.

As excitation wavelength for GCaMP 920 nm was used and emission was detected with a 500-550 nm bandpass filter. mCherry was excited at 1000 nm and emission detected with a 590-630 nm bandpass filter. A 63x magnification water immersion objective with a numerical aperture of 1.0 and a working distance of 2.1 mm (W Plan-Apochromat 63x/1.0, Carl Zeiss, Jena) was used, which resulted in pixel sizes between 300 and 450 nm depending on the region of interest. Images were acquired with a pixel dwell time of at least 2  $\mu$ s and a bit depth of 16 bit, leading to frame rates of 3-5 Hz. The recordings were limited to a maximum duration of two minutes to prevent overheating of the sample.

## 2.2 PREPARATION

The preparation of the flies for calcium imaging was adopted from Kamikouchi, Wiek, et al., 2010. 1-4 days after eclosion, the fly was glued to a coverslip at its thorax and wings with a low-melting point wax mixture of dental wax (Deiberit 502, Siladent, Goslar), oil-based modeling clay (“fantasia Knet”, Carl Weible KG, Schorndorf) and myristic acid (Sigma-Aldrich). The legs were immobilized with a drop of wax and the position of the head was adjusted to line up the rotational axis of the funiculus perpendicular to the coverslip. To reduce muscle-induced motion of the antenna, the scape and pedicel were glued to the head capsule with UV-curing dental glue (Kentoflow, Kent Dental).

To achieve a better match of refractive indices from the objective to the JO neurons, the air gap between pedicel and coverslip was bridged with a drop of glycerol (Sigma-Aldrich). As a biasing electrode for electrostatic displacement of the arista, a 100  $\mu\text{m}$  diameter 100  $\mu\text{m}$  silver wire was inserted into the thorax and stabilized with a drop of wax.

The coverslip was fixed in a 3D-printed plastic holder, which was mounted on a magnetic stand as described in Gras, 2014. The magnetic stand allowed tilting and rotation of the sample under the microscope to align the JO neurons to the focal plane (Fig. 2.1).

## 2.3 STIMULATION

Sinusoidal and sustained deflections of the arista were induced via electrostatic forcing as described in Albert et al., 2007. The animal itself was charged to a bias potential of -40 V via the implanted silver electrode. Two tungsten wires (etched to ca. 50  $\mu\text{m}$  diameter) served as displacement electrodes and were positioned anterior and posterior of the arista with a modified two-axis micropositioner (Narishige). The micropositioner was placed on the same magnetic stand as the coverslip to keep the electrode positions constant while tilting and rotating the preparation. Charge was applied to the electrodes with a high voltage electrostatic displacement controller which modulated the electrode voltage according to a stimulus input signal. The anterior electrode’s charge was modulated with opposing polarity to the posterior one, leading to a push/pull deflection of the arista and more symmetric sinewave displacement. The stimulus input signals were generated with a Micro1401-3 DAQ system and its control software Spike2 (Cambridge Electronic Devices).

Unless otherwise specified, the sine wave stimuli consisted of a 30 s pre-stimulus phase and three repetitions of a 5 s stimulus followed by a 25 s break. The stimulation was frame-synchronized to the microscope data acquisition to allow precise averaging of the stimulus repetitions. As the microscope software allows no user-defined frame intervals, the frame-synchronization led to stimulus durations being a multiple of the frame intervals and not precisely 5 s (usually within 5 s $\pm$ 0.2 s).

For stimulus-response curves the sine wave amplitude was changed in 6 dB steps, covering a range from  $\pm 60$  nm to  $\pm 18$   $\mu\text{m}$  peak-to-peak displacement at

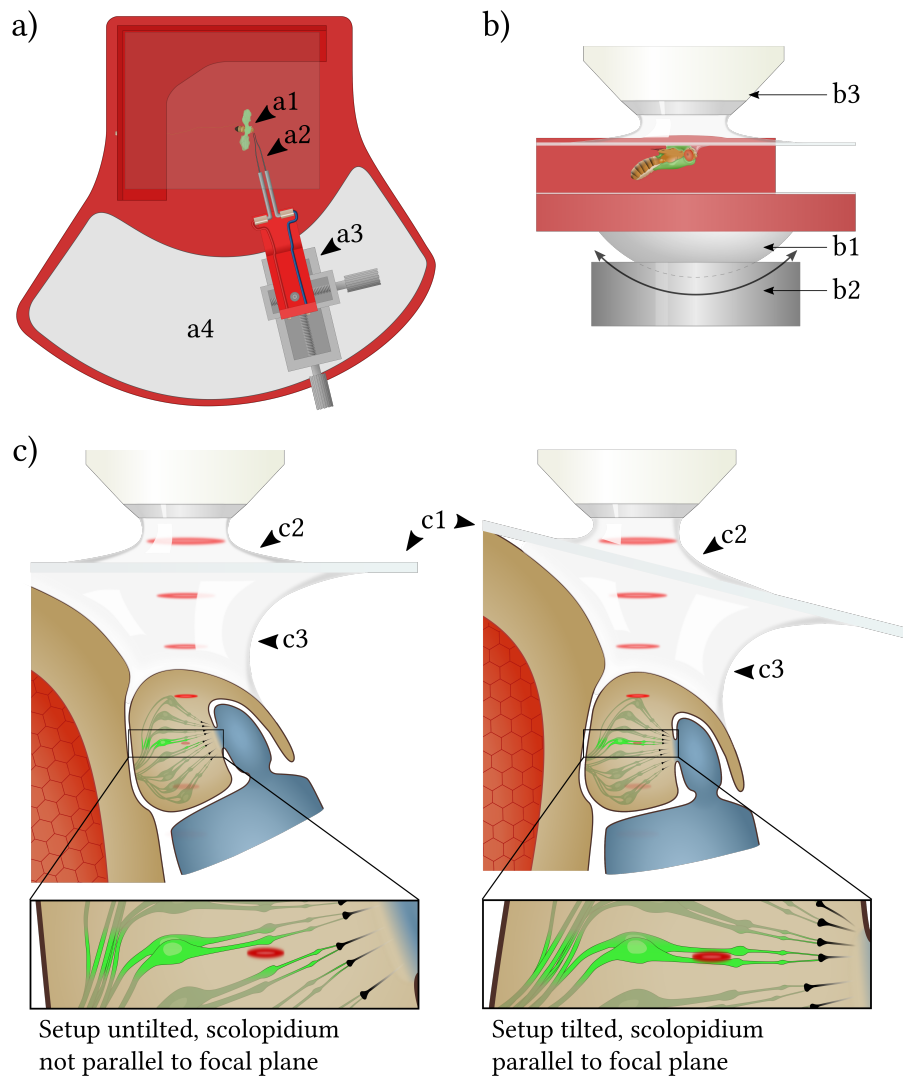


Figure 2.1: FLY HOLDER (a) Topview of the fly holder. The fly is fixed below a coverslip with a low-melting point wax mixture (a1) and the coverslip is mounted on the plastic animal holder with beeswax. Two parallel tungsten electrodes (a2) are placed anterior and posterior of the arista with a micropositioner (a3), which is secured on a metal sheet (a4) with magnetic foil. (b) Side view of the animal holder (micropositioner not shown). The plastic animal holder is attached to a spherical steel cap (b1), which is suspended on a concave magnetic base (b2). The whole animal holder can thus be rotated and tilted relative to the microscope objective (b3) to align the scolopidia of interest to the focal plane. Since the deflection electrodes are tilted as well, their position to the arista remains constant. (c) Alignment of the JO scolopidia. Left panel: Orientation of the JO at the horizontal position of the coverslip (c1). Only the cellbodies and the proximal part of the cilia are in the focal plane, some fluorescence would be detected from the apical cilia of different scolopidia. Right panel: Orientation of the JO after tilting the animal holder. The whole scolopidium is now in the focal plane and signals from the whole dendrite can be detected. As a drawback, the lightpath through the immersion water (c2) and glycerol (c3) becomes asymmetric.

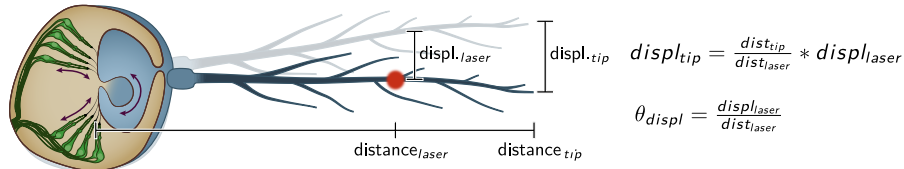


Figure 2.2: EXTRAPOLATION OF TRUE TIP DISPLACEMENT The arista displacement detected by the vibrometer was extrapolated to tip displacement via the ratio of the distances from the tip and the laser point to the antenna’s rotational axis. As a laser position-independent measure the angular displacement in radians can be calculated using the small angle approximation.

the tip of the arista. The displacement of the arista was measured with a Laser Doppler Vibrometer (Polytec, OFV-534 compact sensor head), which was also used to measure the free fluctuation power spectra of the antenna as an indicator of the JO’s condition during the experiments (Göpfert et al., 2003). Because the vibrometer’s 633 nm HeNe laser was detected by the microscope’s photomultipliers even with 500-550 nm GFP emission filters, the displacement for each stimulus intensity could not be measured during the actual experiment but was recorded afterwards. The different stimulus intensities were presented in random order and the vibrometer output was recorded with Spike2 via the Micro1401-3 DAQ system. Since the vibrometer focus was usually not stable at the very fine tip of the arista, the displacement was measured more proximal. To determine the true tip displacement, a picture of the arista and the laser focus was taken with the vibrometer’s camera and its distance to the rotational axis of the funiculus measured with an ImageJ macro. From the distance and the length of the arista the true tip displacement was then extrapolated.

## 2.4 DATA ANALYSIS

### 2.4.1 Image processing

Processing and analysis of the image data was performed in Fiji (Schindelin et al., 2012). The image stacks were filtered with a 3D Gaussian blur to reduce high frequency noise (x, y, z-sigma of 0.8). If obvious sample motion occurred during the experiments, the TurboReg plugin was used to perform a rigid body registration (Thévenaz et al., 1998). After filtering, stimulus repetitions were averaged and  $\Delta F/F_{\text{base}}$ -stacks were calculated. As  $F_{\text{base}}$ -image an average of the five frames before stimulus begin was used, which was then pixel-wise subtracted from the average of the last five frames of the stimulus to obtain  $\Delta F$ -stacks. Region of Interest (ROI) for analysis were selected manually around the cilia of the JO neurons and the average  $\Delta F/F_{\text{base}}$ -values in these ROIs were measured with Fiji’s MultiMeasure plugin and exported for further processing in Python (<http://www.python.org>).



### 2.4.2 Fits and cluster analysis

Nonlinear least square fits of the stimulus-response curves to a four parameter logistic equation of the form  $y = b + \frac{a-b}{1+(x/c)^d}$  were calculated using the Python libraries NumPy (Walt et al., 2011) and Lmfit (Newville et al., 2014). Via the resulting fit parameters the displacement was calculated at which the strongest responding unit would have reached its half-maximal response. For all other units, the corresponding fit amplitude at this displacement was calculated and served together with the slope of the individual fits as clustering parameters. K-means clustering was performed for k values 2 and 3 using the Python library Scikit-learn (Pedregosa et al., 2012). The resulting cluster sets were scored according to their average silhouette value (Rousseeuw, 1987), and the k value better describing the grouping was used for color coding the stimulus-response curves and corresponding fits.

$\Delta F$ -signals from different subcellular regions were fitted to single- and bi-exponential functions of the form  $y = a * (1 - e^{-x/\tau}) + c$  and  $y = a_1 * (1 - e^{-x/\tau_1}) + a_2 * (1 - e^{-x/\tau_2}) + c$ .

## 2.5 FLIES

Flies were kept in a 12 h/12 h light/dark-cycle at 25°C and 60% air humidity. They were raised on food made of apple juice, flour, sugar, yeast, agar, salt, water and propionic acid. The following fly genotypes were used for calcium imaging experiments:

$w^{1118}; n\text{-syb-LexA::p65/CyO}; lexAop\text{-GCaMP6m}/lexAop\text{-GCaMP6m}$

For stimulus-response curves and initial imaging experiments, GCaMP6m was expressed in all neurons under the control of n-syb-LexA.

Fly lines used:

- $w^{1118}; P\{y^{+t7.7}w^{+mC}=13XLexAop2\text{-IVS-GCaMP6m-p10}\}su(Hw)attP1$   
Bloomington stock number: 44275
- $y^1w^s; PBac\{y^{+mDint2}w^{+mC}=n\text{-Syb-lexA::p65}\}VK00018/CyO,$   
 $P\{Wee\text{-P.ph0}\}Bacc^{Wee\text{-P20}}; Dr^1/TM6C, Sb^1Tb^1$   
Bloomington stock number: 52247

$w^{1118}; n\text{-syb-LexA::p65/UAS-6XmCherry}; lexAop\text{-GCaMP6m}/JO15\text{-GAL4}$

To identify sound-sensitive neurons after the experiment, JO15-GAL4 was used to express hexameric mCherry in most A/B neurons.

Fly lines used:

- $w^{1118}; P\{y^{+t7.7}w^{+mC}=13XLexAop2\text{-IVS-GCaMP6m-p10}\}su(Hw)attP1$   
Bloomington stock number: 44275

- $y^1w^*$ ; PBac{y<sup>+mDint2</sup>w<sup>+mC</sup>=n-Syb-lexA::p65}VK00018/CyO, P{Wee-P.ph0}Bacc<sup>Wee-P20</sup>; Dr<sup>1</sup>/TM6C, Sb<sup>1</sup>Tb<sup>1</sup>  
Bloomington stock number: 52247
- $y^1w^*$ ; PBac{20XUAS-6XmCherry-HA}VK00018/CyO, P{Wee-P.ph0}Bacc<sup>Wee-P20</sup>; Dr<sup>1</sup>/TM6C, Sb<sup>1</sup>Tb<sup>1</sup>  
Bloomington stock number: 52267
- $w^*$ ; P{w<sup>+mC</sup>=J21.17-GAL4}JO15/TM3, Sb<sup>1</sup>  
Bloomington stock number: 6753

*iav*<sup>1</sup>; *n-syb-LexA::p65/+* ; *lexAop-GCaMP6m/+*

For calcium imaging in *inactive* mutants, GCaMP6m was expressed in all neurons under the control of *n-syb-LexA*.

Fly lines used:

- $w^{1118}$ ; P{y<sup>+t7.7</sup>w<sup>+mC</sup>=13XLexAop2-IVS-GCaMP6m-p10}su(Hw)attP1  
Bloomington stock number: 44275
- $y^1w^*$ ; PBac{y<sup>+mDint2</sup>w<sup>+mC</sup>=n-Syb-lexA::p65}VK00018/CyO, P{Wee-P.ph0}Bacc<sup>Wee-P20</sup>; Dr<sup>1</sup>/TM6C, Sb<sup>1</sup>Tb<sup>1</sup>  
Bloomington stock number: 52247
- *iav*<sup>1</sup>;+;+ (*inactive*-mutation, Q<sub>455</sub>stop)

$w^{1118}$  ; *nompC*<sup>3</sup>/*nompC*<sup>3</sup> ; NP0761-GAL4/UAS-GCaMP6m

For calcium imaging of all JO neurons in *nompC* mutants, UAS-GCaMP6m was expressed under the JO-wide driver NP0761-GAL4 (Hayashi et al., 2002; Kamikouchi et al., 2006).

Fly lines used:

- $w^{1118}$ ; *nompC*<sup>3</sup> *cn<sup>1</sup>bw<sup>1</sup>*/CyO (*nompC*-null mutation, K<sub>747</sub> stop)  
Bloomington stock number: 42258
- $w^{1118}$ ; PBac{y<sup>+mDint2</sup>w<sup>+mC</sup>=20XUAS-IVS-GCaMP6m}VK00005  
Bloomington stock number: 42750
- $w^{1118}$ ; CyO/Sp ; NP0761-GAL4/TM6B, Sb<sup>1</sup>Tb<sup>1</sup>

$w^{1118}$  ; *nompC*<sup>3</sup>/*nompC*<sup>1</sup> ; *JO15-GAL4/UAS-GCaMP6m*

For calcium imaging of sound-sensitive neurons in *nompC* mutants, UAS-GCaMP6m was expressed under control of the subgroup A/B-driver JO15-GAL4 (Hayashi et al., 2002; Kamikouchi et al., 2006).

Fly lines used:

- $w^{1118}$ ; *nompC*<sup>3</sup> *cn<sup>1</sup>bw<sup>1</sup>*/CyO (*nompC*-null mutation, K<sub>747</sub> stop)  
Bloomington stock number: 42258

- *nompC<sup>1</sup>cn<sup>1</sup>bw<sup>1</sup>/CyO* (*nompC*-null mutation, K<sub>760</sub> stop)  
Bloomington stock number: 42260
- *w<sup>\*</sup>; P{w<sup>+mC</sup>=J21.17-GAL4}JO15/TM3, Sb<sup>1</sup>*  
Bloomington stock number: 6753

## 2.6 SCANNING ELECTRON MICROSCOPY

The scanning electron micrograph shown in Figure 1.1 was acquired on a Hitachi TM3000 tabletop microscope during a public demonstration of the microscope by the German Federal Ministry of Research and Education. The sample head was cut from a cold-anesthetized fly and immediately scanned without fixation in low vacuum. The image was manually stitched from three single images and adjusted for contrast by histogram equalization.



## RESULTS

---

### 3.1 COMPARISON BETWEEN SINGLE-PHOTON EXCITATION WIDEFIELD IMAGING AND TWO-PHOTON SCANNING MICROSCOPY DATA

GCaMP6-signals evoked in the JO neurons by sinusoidal stimulation are robustly detected by both imaging systems over a broad range of arista tip displacements, from very small stimulus amplitudes below  $\pm 100$  nm to large deflections of  $\pm 20000$  nm. The widefield imaging system reaches better signal to noise ratios, which is due to the larger amount of collected emission light and the higher sensitivity of the EMCCD camera compared to the scanning microscope's photomultipliers. In turn, the single photon excitation leads to stronger overall photobleaching (Fig. 3.1).

To reduce the influence of noise on the calculated relative fluorescence changes, three repetitions of each sine stimulus were averaged. In addition, a 3D Gaussian blur was applied as a low-pass filter to reduce high-frequency noise (Fig. 3.1d, lower trace).

The spatial resolution achieved by two-photon excitation scanning microscopy allows separation of individual scolopidia in the JO, whereas the images acquired with a widefield single photon excitation system show the blurry fluorescence of all scolopidia at once. To reach frame rates of 5 Hz when scanning whole JO slices, the pixel resolution had to be strongly reduced, which only allowed the distinction of individual scolopidia instead of individual sensory neurons. In most cases though, the distance between individual neurons in the scolopidia is smaller than the theoretical optical resolution of the microscope (around 500 nm), setting the resolution limit for diffraction-limited imaging systems to receptor units rather than sensory neurons.

Despite the restriction to scolopidia, the increase in resolution compared to the formerly used calcium imaging and electrophysiological recording methods is a significant improvement and allows the spatial localization of calcium signals within the JO receptor units without resorting to single-cell labeling methods like flipout-mediated expression of GCaMP.

### 3.2 RESPONSE OF RECEPTOR UNITS TO ARISTA DEFLECTION

#### 3.2.1 *Sinusoidal stimulation*

Applying sinusoidal deflection to the arista to mimic sound stimuli elicits fluorescence signal increases in the JO receptor units, as shown before by Kamikouchi et al., 2009 and Effertz et al., 2011. Depending on stimulus strength and the cellular compartment used as a ROI, the calcium signal rises within several 100 ms after stimulus onset and takes up to 15 s to decay back to baseline. The sensitivity of the receptor units varies greatly: The most sensitive recep-

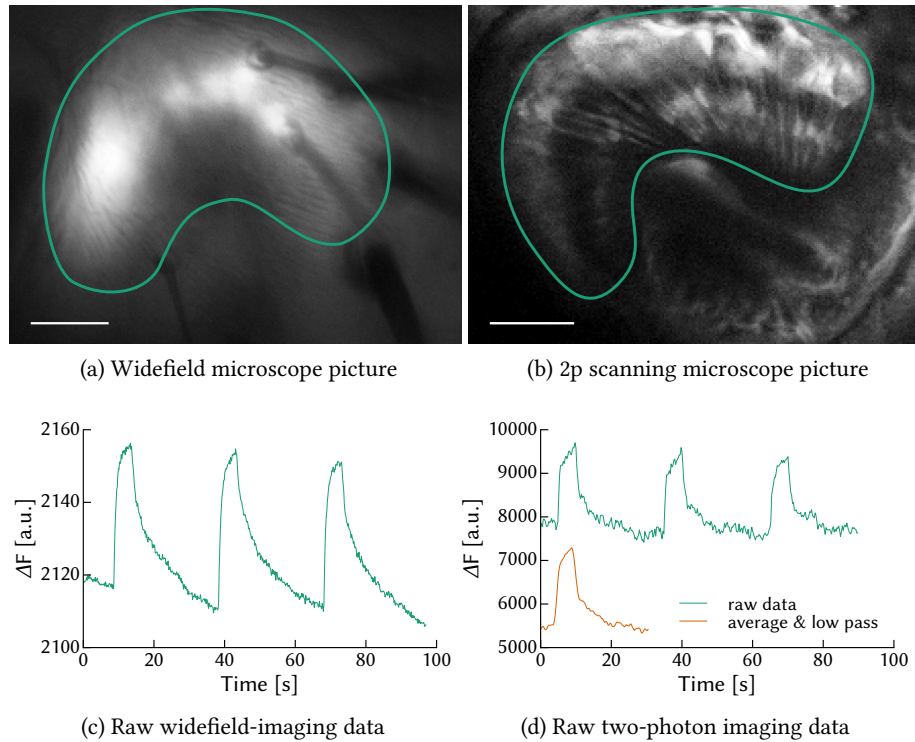


Figure 3.1: COMPARISON BETWEEN SINGLE- AND TWO-PHOTON EXCITATION IMAGING Response of two JOS to three repetitions of a sine stimulus with an arista tip displacement amplitude of  $\pm 1 \mu\text{m}$  in a ROI covering all scolopidia (in the case of two-photon excitation, all scolopidia in one optical slice). (a,c) Data from widefield system, unfiltered raw trace (b,d) Data from two-photon scanning microscope, upper trace: unfiltered raw data, lower trace: upper trace averaged and low-pass filtered with a gaussian blur ( $\sim 2500$  a. u. to separate traces). The absolute values are in arbitrary units (a.u.) and are not comparable between the systems due to different photon number—pixel value conversion functions of the EMCCD camera and the photomultipliers of the scanning microscope. Scalebars:  $20 \mu\text{m}$ , fly genotype:  $w^{1118}; n\text{-syb-LexA}::p65/\text{CyO}; \text{lexAop-GCaMP6m}/\text{lexAop-GCaMP6m}$  ( $\sigma^7$ )

tor units robustly respond to arista tip displacements as small as 50 nm, while others hardly respond below a displacement of 5000 nm. All measured receptor units did not show long-term adaptation to sinusoidal stimulation, which is consistent with the tonic firing measured in antennal nerve recordings. The millisecond-range adaptation during step displacement of the arista observed by Albert et al., 2007 can not be resolved with the used calcium sensor and the imaging speed of 3.5–5 Hz.

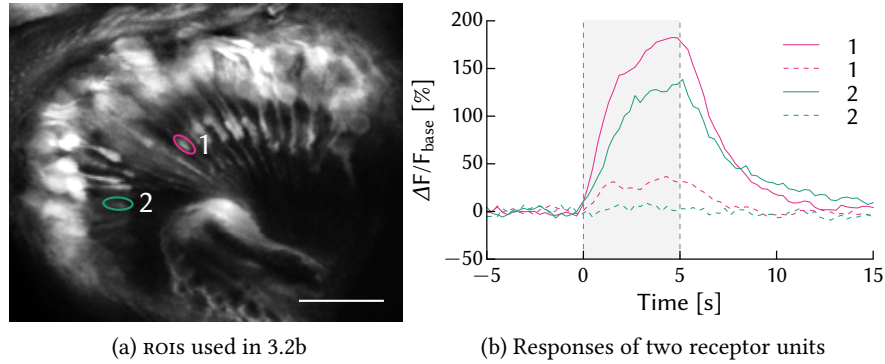


Figure 3.2: SENSITIVITY DIFFERENCES BETWEEN INDIVIDUAL RECEPTOR UNITS Example responses of two receptor units to a 5 s sine stimulus with a tip displacement of 13.4  $\mu\text{m}$  (solid line) and 140 nm (dashed line). Grey area marks stimulus duration, scalebar: 20  $\mu\text{m}$ , fly genotype:  $w^{1118}$ ;  $n\text{-syb-LexA}::p65/CyO$ ;  $\text{lexAop-GCaMP6m/lexAop-GCaMP6m}$  ( $\sigma$ )

### 3.2.2 Mixed stimulation

When a 2.5  $\mu\text{m}$  prestep is added to  $\pm 5 \mu\text{m}$  sinusoidal deflection, most receptor units respond to both the sustained and sinusoidal component of the stimulus, although with very different ratios (Fig. 3.3b). Most receptor units show a much stronger calcium response to the sinusoidal part of the stimulus, though some completely reject one of the stimulus components and respond only to either the prolonged offset (Fig. 3.3c) or the alternating sine stimulation (Fig. 3.3a). The JO receptor units thus seem to form stimulus filters, with characteristics ranging from strong high-pass to equally strong low-pass.

## 3.3 SIGNAL DYNAMICS WITHIN RECEPTOR UNITS

Comparison of the calcium signals in subcellular regions of the receptor units shows differences in the time course of the measured fluorescence change (Fig. 3.4). Whereas in the distal region of the scolopidia the signal rises quickly after the stimulus onset and reaches a plateau level after 1 s, the fluorescence change happens much more gradual in the proximal part of the dendrites and usually does not reach a plateau value during the 5 s stimulus. In the cell bodies, the signal rises quickly within the first 0.5 s and then continues with a slower increase during the 5 s stimulus, while in the axonal region of the

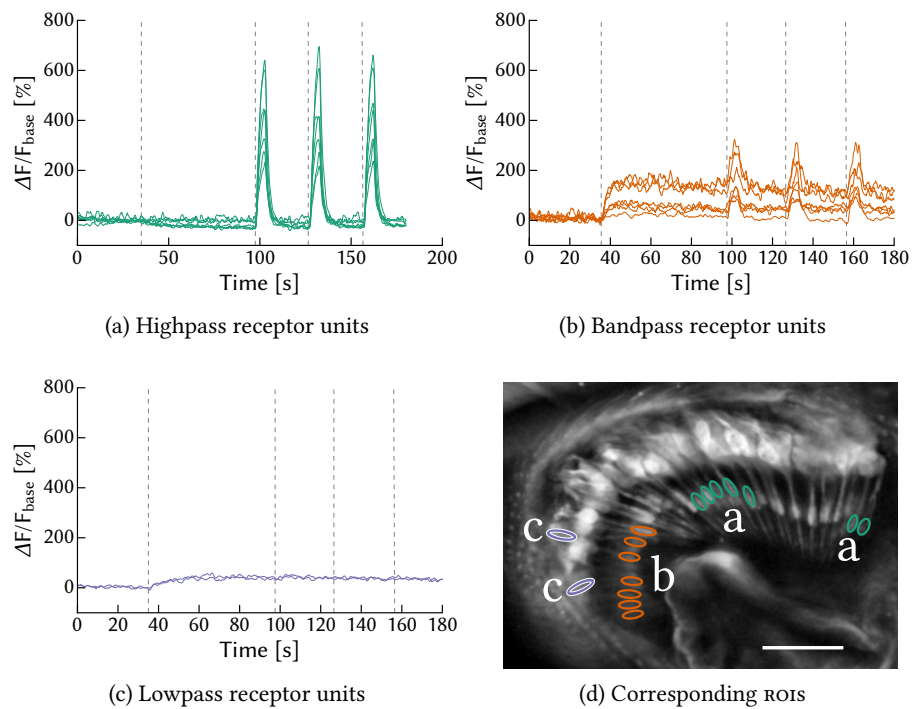


Figure 3.3: JO RECEPTOR UNIT RESPONSE TO MIXED STIMULATION (a, green) Highpass-units which show almost no response to the sustained deflection (b, orange) Bandpass-units which respond to both stimulus components (c, purple) Lowpass-units which show no response to sinusoidal deflection (d) ROIs plotted in a, b, and c. Dashed lines mark step and sine stimulus onset. Scalebar: 20  $\mu\text{m}$ , fly genotype: *w<sup>1118</sup>*; *n-syb-LexA::p65/CyO*; *lexAop-GCaMP6m/lexAop-GCaMP6m* ( $\sigma$ )



COMPARTMENT	AIC SINGLE EXP.	AIC BI-EXP.	$\tau_{\text{BETTER FIT}}$
Ciliary dilation	243	249	0.34 s
Basal body	257	263	2.5 s
Cell body	272	253	0.27 s, 676 s
Axon	252	258	0.52 s

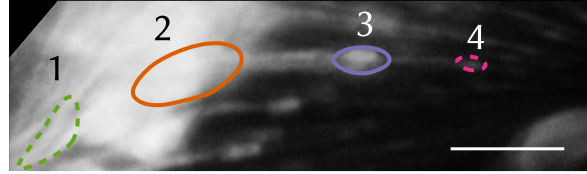
Table 3.1: FIT RESULTS FOR SUBCELLULAR REGIONS SHOWN IN FIG. 3.4 Single- and bi-exponential fits to the  $\Delta F$ -data shown in Fig. 3.4 were evaluated based on the Akaike Information Criterion (AIC), which provides a relative goodness of fit-measure including an overfitting penalty. Lower scores indicate the more sufficient of the two tested models, which only in the case of the cell bodies was the more complex bi-exponential fit. The resulting time constants are shown for the better scoring fit.

neurons the signal time course again resembles the measurements from the distal dendritic region, with a steady plateau fluorescence after 1 s.

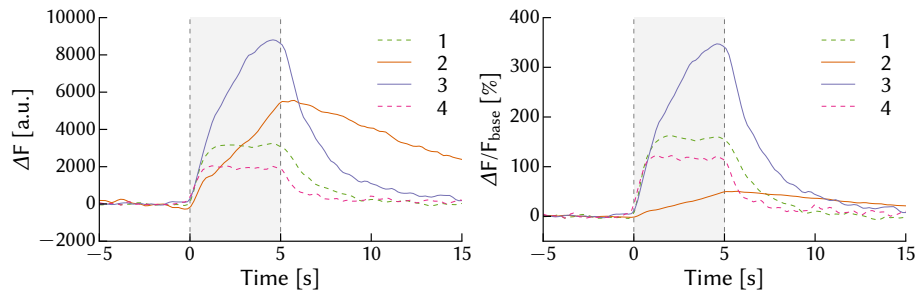
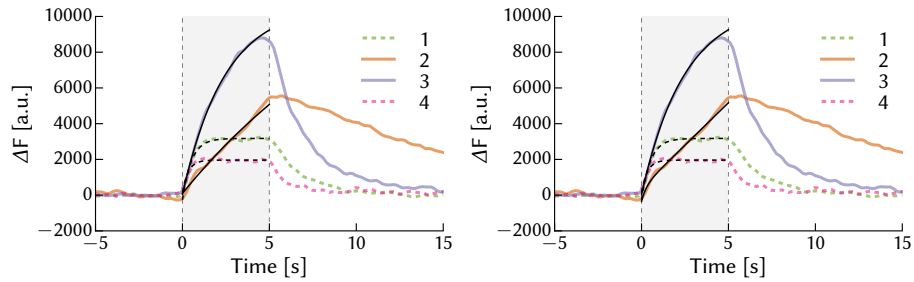
A possible explanation for these different signal dynamics could be the source of the measured calcium concentration increase: The step-like signal in the distal region could arise from actual calcium influx via mechanically gated channels in the dendritic tips alone, whereas especially in the cell bodies also slow calcium- (or membrane potential-) induced calcium release from cell-internal sources such as mitochondria and the endoplasmatic reticulum could contribute to the signal.

The step-like GCaMP-signal in the axons most likely results from fast calcium influx via voltage-gated cation channels, triggered by the membrane potential change induced by the mechanical stimulus. As the spike rate of the JO neurons stays constant during extended sine stimuli, this tonic calcium signal seems to closely resemble the membrane potential (with the slow initial increase owed to the slow reaction time of the calcium sensor).

To further characterize the fluorescence signals shown in Fig. 3.4, exponential and bi-exponential functions were fitted to the time traces during the stimulus, similar to Storace et al., 2015 (fits overlayed in 3.4d and 3.4e). The signals at the ciliary dilations, basal bodies and axons are well fitted by a single exponential increase, whereas based on the Akaike Information Criterion (AIC) (Akaike, 1974), the signal at the cell body is better fitted by a bi-exponential function, with one time constant similar to the other compartments and a second, larger one (see table 3.1 for results). This fit result would support the involvement of two processes in the calcium concentration increase at the cell body, in which case it might mirror the mechanotransduction currents even less directly than calcium imaging in general. As the cell bodies are usually difficult to tell apart at the achieved z-resolution and to circumvent the influence of a possible additional source of calcium, in further experiments ROIs to measure receptor unit activity were chosen in dendritic regions.



(a) ROIs used for 3.4b and 3.4c

(b) Absolute fluorescence change ( $\Delta F$ )(c) Relative fluorescence change ( $\Delta F/F_0$ )

(d) Single exponential fits of 3.4b

(e) Double exponential fit of 3.4b

Figure 3.4: SIGNAL DYNAMICS WITHIN SINGLE RECEPTOR UNITS Subcellular regions of JO receptor units show distinct signal dynamics. Whereas signals in axons (1), basal bodies (3) and the ciliary dilation (4) are best fit by a single exponential increase (3.4d), the fast onset and slow signal component during the stimulus at the cell body (2) are best fitted with a double exponential increase (3.4e). Scalebar= $10\ \mu\text{m}$ , example fly genotype:  $w^{1118}$ ;  $n\text{-syb-LexA}::p65/CyO$ ;  $lexAop\text{-GCaMP6m}/lexAop\text{-GCaMP6m}$  ( $\sigma$ ).

### 3.4 INTENSITY-RESPONSE CURVES

As shown in Fig. 3.2, the JO receptor units show differences in response sensitivity to sinusoidal stimulation. To compare the sensitivities of multiple units, intensity-response curves were created from calcium signal responses to sinusoidal stimulation between  $\pm 50$  and  $\pm 20000$  nm of all distinguishable units in an optical slice. From the measured time traces, the average of the last five frames before the end of the stimulus was calculated and plotted for all measured intensities. The response curves of three successfully measured animals are shown in Fig. 3.5a, c, e.

#### 3.4.1 Differences to electrophysiology data

The response curves show several interesting differences to antennal nerve field potential recordings and the whole-cell voltage clamp JO-spike recordings at the GFN performed by Lehnert et al., 2013. While these recordings showed a clear response plateau level and a subsequent response decline, the calcium signals in Fig. 3.5 in most cases keep increasing monotonically up to the highest stimulus intensities (sometimes leading to a slight plateau), thus stronger resembling the stimulus-generator current curves recorded by Lehnert et al., 2013. In addition, the stimulus range eliciting the strongest calcium signal increase is around ten times larger than measured by Effertz et al., 2011 and two times larger than observed by Lehnert et al., 2013. This apparent overall sensitivity difference might be due to the different recording methods and calcium sensors used in the studies, even though under this assumption different minimum response thresholds would be expected, which instead are similar in all studies.

#### 3.4.2 Receptor unit subgroups

The resulting curves show highly variable response characteristics, with response thresholds between  $\pm 50$  and  $\pm 5000$  nm and maximum responses between 50 and more than 700 % relative fluorescence increase. An interesting property which could not be resolved with the group recording/imaging methods employed in former studies are the different slopes of the traces. Signals of receptor units with low response thresholds seem to increase with a comparatively shallow slope, thus encoding a wide displacement range. Other units instead reach similar maximum responses, but begin to respond at much higher displacements and therefore seem to compress their encoded information into a smaller stimulus range. A third group distinguishable in all measured flies only responds to very high stimulus amplitudes above  $\pm 3000$  nm and reaches maximal responses below 300% relative increase in the applied stimulus range.

Since this observation might correspond to the sound- and wind-sensitive receptor unit subgroups proposed by Kamikouchi et al., 2009 and Yorozu et al., 2009, cluster analysis was done to quantify potential response curve grouping.

To obtain parameters usable for clustering, fits of the calcium signal response curves to a four parameter logistic equation were created as calculated by Effertz et al., 2011. From the fits, the response of each unit at the displacement which elicited the half-maximal response of the strongest responding receptor unit was calculated. These values together with the slope parameter of each fit were used for k-means clustering.

The k-means clustering was performed once with an estimated cluster number of two, corresponding to one sensitive and one insensitive subgroup and three, to test for possible further subdivision of the more sensitive neurons. The resulting clusters were scored with the silhouette criterion and the higher scoring k values were used for color-coding the fits shown in Fig. 3.5b, d, f (Rousseeuw, 1987). Only in one of the three flies three groups of response curves scored slightly higher than two groups (Fig. 3.5d).

Performing a whitening transformation on the data used for clustering to account for the non-circular clusters strongly reduces the separation of the detected clusters and leads to the detection of less meaningful clusters even for  $k=2$ , indicating that the data is unsuited for the k-means algorithm. The results of the cluster analysis thus might be quite different using an algorithm able to work with non-spherical clusters of different sizes and densities, as they are present in these response curves.

### 3.4.3 Response of subgroup A/B-neurons

In addition to the cluster analysis, a double labeling approach was used to further investigate whether the different receptor unit sensitivities observed in the intensity-response curves are related to the proposed subgroups of the JO. LexAop-GCaMP6m was expressed in the whole JO via an n-syb-LexA driver line. In addition, JO15-GAL4, one of the GAL4-lines described by Kamikouchi et al., 2006, was used to label most of the putative sound-sensitive A/B-neurons with the red fluorescent protein 6XmCherry.

After the imaging experiments, the GCaMP-responses of the A/B-neurons could be identified via the colocalization with mCherry-expression. In contrast to the experiments by Kamikouchi et al., 2009 and Effertz et al., 2011, the information about the response of the receptor units not labeled by JO15-GAL4 was still retained due to the JO-wide GCaMP expression (Fig. 3.7).

The resulting response curves of four double-labeled animals show a clear overlap of the JO15-labeled neurons with high- and intermediate sensitivity units (Fig. 3.8). This is consistent with the widefield imaging and group-ablation results from Kamikouchi et al., 2009 and Effertz et al., 2011, but in addition shows a response variability within the A/B-subgroups. A similar diversity within sound-sensitive receptor units was suspected by Baker, 2015 as a reason for the observed response diversity of auditory interneurons, with the possible physiological use of extending the temporal resolution capabilities of *Drosophila's* auditory system.

K-means clustering of uncorrected data successfully separates A/B and unlabeled neurons into different clusters (Fig. 3.8b, f, h), though with very low scoring differences between  $k=2$  and  $k=3$ . One exception is the fit of Fig. 3.8e,

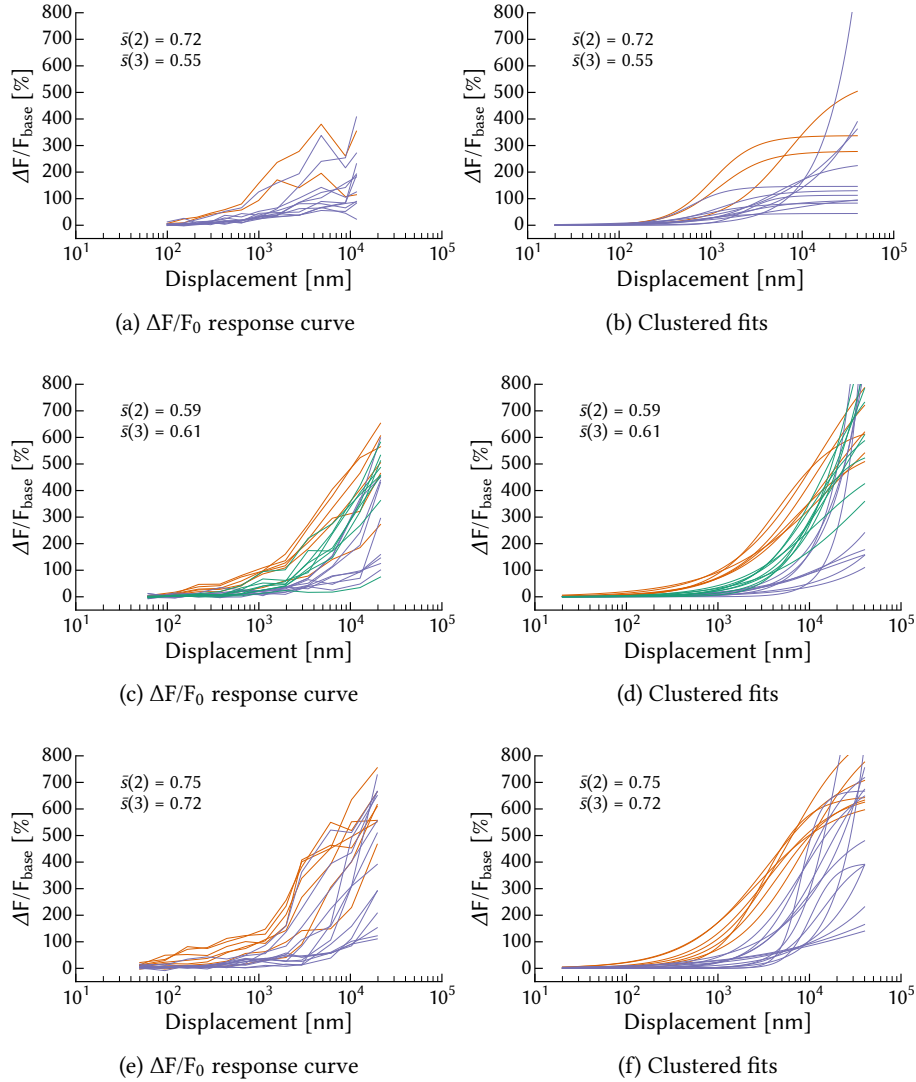


Figure 3.5: CLUSTER ANALYSIS OF JO NEURONS, CLUSTER NUMBER CHOSEN VIA SILHOUETTE CRITERION (a,c,e): Stimulus-response curves of three control flies (b,d,f): Corresponding fits with a four parameter logistic curve. Colors: groups of response characteristics deduced from k-means cluster analysis.  $S(2)$  and  $s(3)$  are the calculated silhouette scores for clustering with  $k=2$  and  $k=3$ , the higher scoring result (closer to 1) was used for color-coding the fits. Fly genotype:  $w^{1118}; n-syb-LexA::p65/CyO; lexAop-GCaMP6m/lexAop-GCaMP6m$  ( $\sigma^7$ )

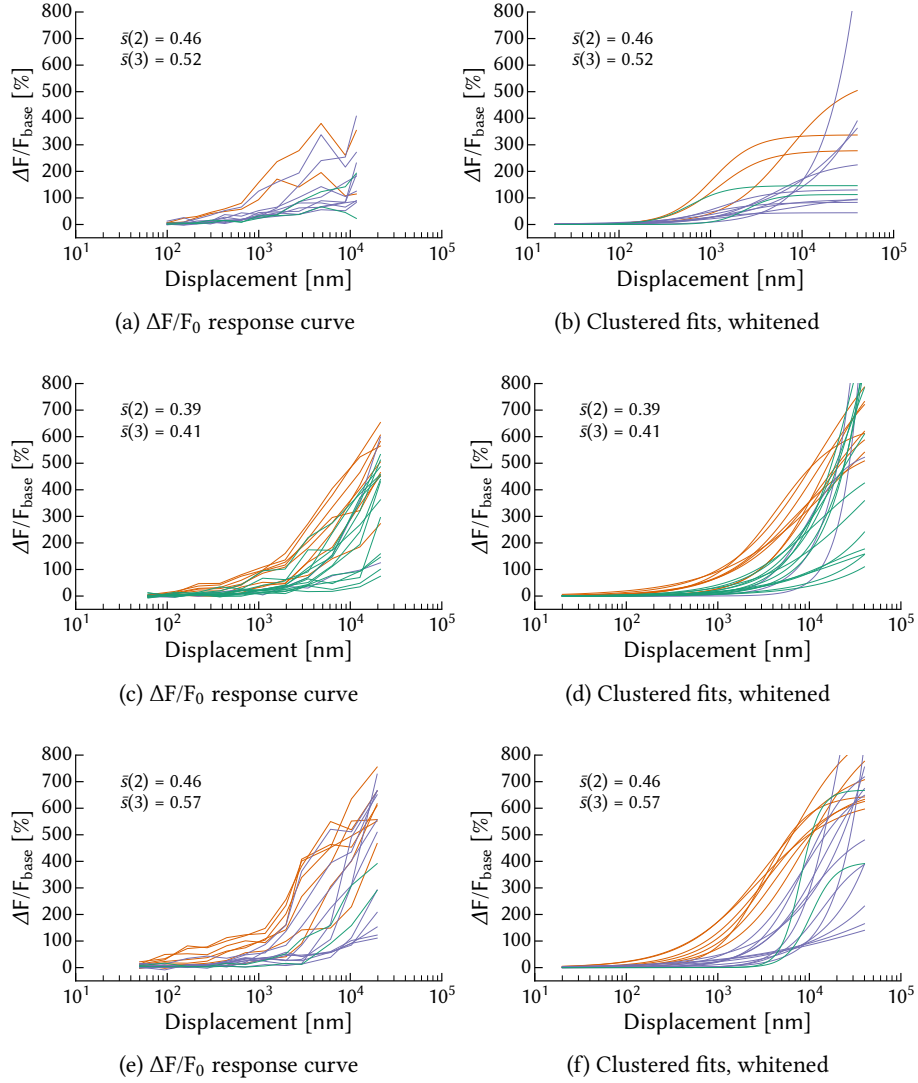


Figure 3.6: CLUSTER ANALYSIS OF JO NEURONS AFTER WHITENING TRANSFORMATION, CLUSTER NUMBER CHOSEN VIA SILHOUETTE CRITERION (a,c,e): Stimulus-response curves of three control flies (b,d,f): Corresponding fits with a four parameter logistic curve. Colors: groups of response characteristics deduced from k-means cluster analysis.  $S(2)$  and  $s(3)$  are the calculated silhouette scores for clustering with  $k=2$  and  $k=3$ , the higher scoring result (closer to 1) was used for color-coding the fits. Fly genotype:  $w^{1118}; n\text{-syb-LexA}::p65/CyO; lexAop\text{-GCaMP6m}/lexAop\text{-GCaMP6m}$  ( $\sigma^3$ )

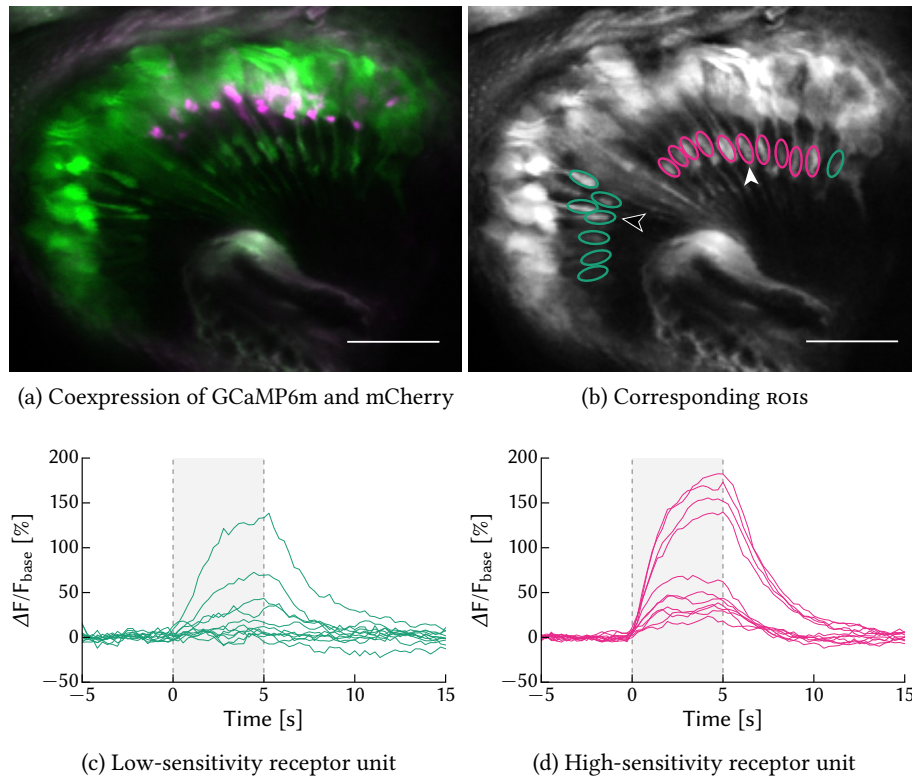


Figure 3.7: LABELING OF A/B NEURONS VIA 6XMCHERRY (a) JO15-Gal4/UAS-6XmCherry labels a subset of the A/B neurons, all other neurons are only expressing GCaMP6m. Scalebar:  $20\mu\text{m}$  (b) ROIs deduced from mCherry- and GCaMP6m expression shown in a. Scalebar:  $20\mu\text{m}$  (c) Response of a low-sensitivity receptor unit to sinusoidal stimulation between 80 and 13000nm, ROI used: black arrow in b. (d) Response of a high-sensitivity, JO15-GAL4 labeled receptor unit to sinusoidal stimulation between 80 and 13000nm, ROI used: white arrow in b. Example fly genotype:  $w^{1118}$  ;  $n\text{-syb-LexA}::p65/UAS\text{-}6XmCherry$  ;  $lexAop\text{-}GCaMP6m/JO15\text{-}GAL4$  ( $\sigma$ )

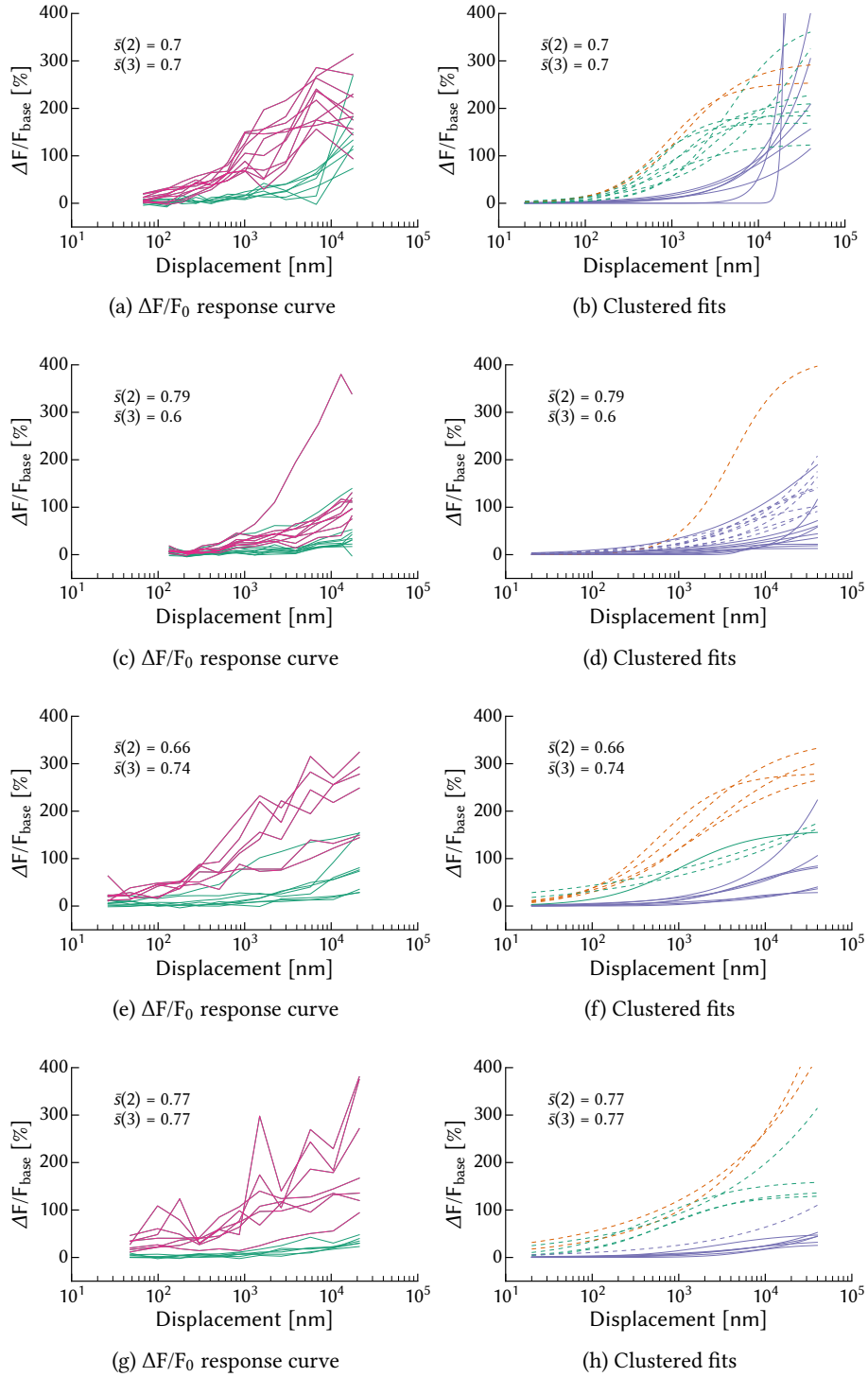


Figure 3.8: CLUSTER ANALYSIS OF MCHERRY-LABELED A/B-NEURONS, CLUSTER NUMBER CHOSEN VIA SILHOUETTE CRITERION (a, c, e, g): Stimulus-response curves of four flies with 6XmCherry-labeled A/B-neurons. Magenta traces: 6XmCherry-expressing units, green traces: units expressing only GCaMP (b, d, f, h): Corresponding fits with a four parameter logistic curve. Trace colors: Groups deduced from k-means cluster analysis, dashed lines indicate fits of 6XmCherry-labeled units.  $S(2)$  and  $s(3)$  are the calculated silhouette scores for clustering with  $k=2$  and  $k=3$ , the higher scoring result (closer to 1) was used for color-coding the fits. Fly genotypes:  $w^{1118}$ ;  $n\text{-syb-LexA::p65/UAS-6XmCherry}$ ;  $lexAop\text{-GCaMP6m}/\text{J015-GAL4}$  ( $\sigma^3$ )



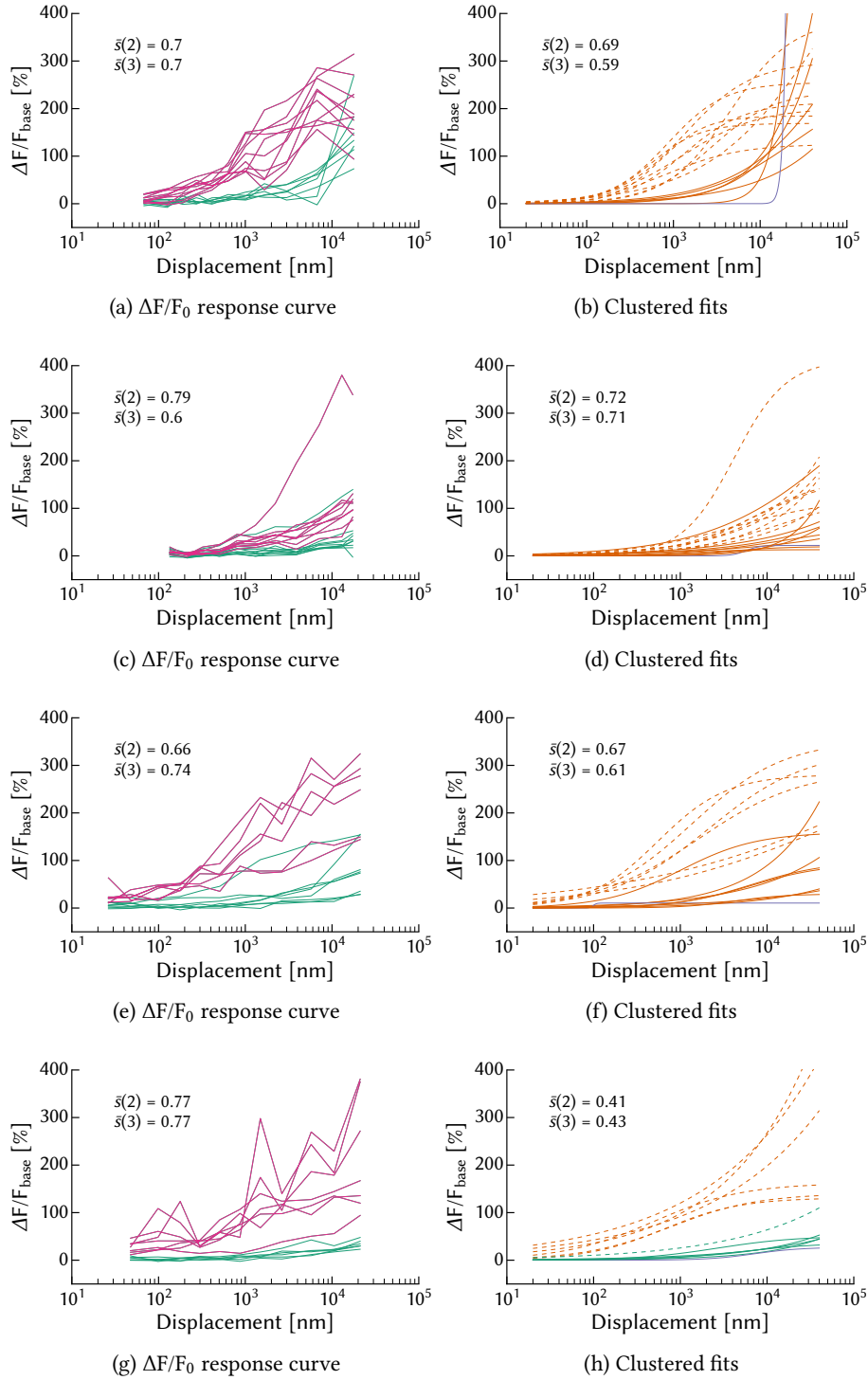


Figure 3.9: CLUSTER ANALYSIS OF MCHERRY-LABELED A/B-NEURONS AFTER WHITENING TRANSFORMATION, CLUSTER NUMBER CHOSEN VIA SILHOUETTE CRITERION (a, c, e, g): Stimulus-response curves of four flies with 6XmCherry-labeled A/B-neurons. Magenta traces: 6XmCherry-expressing units, green traces: units expressing only GCaMP (b, d, f, h): Corresponding fits with a four parameter logistic curve.  $S(2)$  and  $s(3)$  are the calculated silhouette scores for clustering with  $k=2$  and  $k=3$ , the higher scoring result (closer to 1) was used for color-coding the fits. Trace colors: Groups deduced from  $k$ -means cluster analysis, dashed lines indicate fits of 6XmCherry-labeled units.  $S(2)$  and  $s(3)$  are the calculated silhouette scores for clustering with  $k=2$  and  $k=3$ , the higher scoring result (closer to 1) was used for color-coding the fits. Fly genotypes:  $w^{1118}; n-syb-LexA::p65/UAS-6XmCherry; lexAop-GCaMP6m/\text{JO15-GAL4}$  ( $\sigma^r$ )

which results in three plausible clusters. After correction for equal variance and non-circular clusters, even the separation into two groups only is only successful in one fly (Fig. 3.8h).

### 3.5 INACTIVE MUTANTS

Based on the complete lack of sound-induced currents in the GFN in *inactive* mutants compared to the remaining currents in *nompC* flies, Lehnert et al., 2013 propose Inactive to be the primary transduction channel of the JO's A/B neurons instead of NompC. This conclusion differs from the results of Wiek, 2013, who could detect sound-induced calcium signals in the JO of *inactive* mutants, and to some extent contradicts the phase-locked overamplification in these flies, which inherently requires information about the stimulus and thus mechanosensation (though not necessarily directly via a channel protein).

A possible explanation for these differing results might again be found in the used recording methods. Whereas Lehnert et al., 2013 measured the downstream signal at the GFN, which besides mechanotransduction also requires signal propagation along the antennal nerve, Wiek, 2013 measured calcium increase directly at the dendrites and cell bodies of the JO. Therefore, the calcium imaging could have detected mechanically induced calcium currents at the dendrites that would be invisible at the GFN, if the *inactive* mutation only impairs signal propagation within the cells rather than the initial mechanotransduction event.

The whole-JO imaging though did not provide sufficient information on the precise origin of the calcium signals due to light scattering and the overlay of all JO cells. To acquire more detailed information about the origin of the remaining calcium signals in *inactive* mutants, the imaging experiments were repeated with two-photon calcium imaging. The method is particularly well suited for these experiments due to its ability to precisely localize the spatial origin of fluorescence with a resolution sufficient to distinguish subcellular compartments in the JO.

#### 3.5.1 Dendritic signals in *inactive* mutants

Flies expressing *lexAop-GCaMP6m* under control of an *n-syb-LexA* driver were used for JO-wide expression in male *inactive* mutant flies. In one of the nine successfully measured flies small stimulus-evoked fluorescence signals with a maximum relative fluorescence increase of 30 % were observed at the distal tips of a few receptor units (Fig. 3.10a, ROIs 1). The signals were only distinguishable from background noise at high displacement amplitudes above  $\pm 10 \mu\text{m}$  and about a factor of 5 smaller than signals in similar regions of non-mutant flies (see Fig. 3.4 on page 24 for comparison). The origin of the signals in the dendrites distal of the ciliary dilation corresponds to the localization of NompC, as shown by Lee et al., 2010.

In a second fly, even smaller fluorescence signals were visible in more proximal dendrite regions between basal- and cell body (Fig. 3.11). The signals

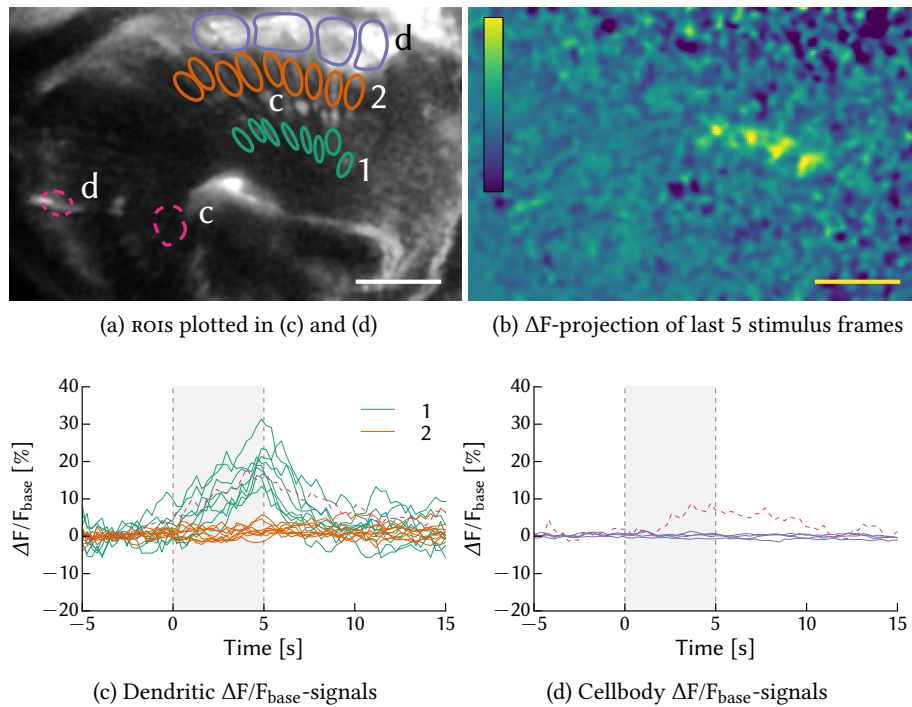


Figure 3.10: REMAINING CALCIUM SIGNALS IN *INACTIVE* MUTANTS, I In one of the measured flies, calcium signals were visible only in the distal, but not in the more proximal region of the dendrites in the same optical slice. Another small signal was detected at one cell body (a, ROI d) (a) ROIs plotted in (c) and (d), 1: distal ROIs, 2: proximal ROIs. Scalebar=20  $\mu\text{m}$  (b) Average of last five stimulus frames of  $\Delta F$ -data,  $\Delta F$  calibration bar: -500–700 [a.u.], scalebar=20  $\mu\text{m}$  (c)  $\Delta F/F_{\text{base}}$ -timetraces of distal and proximal dendritic ROIs (d)  $\Delta F/F_{\text{base}}$ -timetraces of several cellbodies. Stimulus amplitude: +/- 10  $\mu\text{m}$ , fly genotype: *iav*<sup>1</sup>; *n-syb-LexA::p65/+*; *lexAop-GCaMP6m/+* ( $\sigma$ )

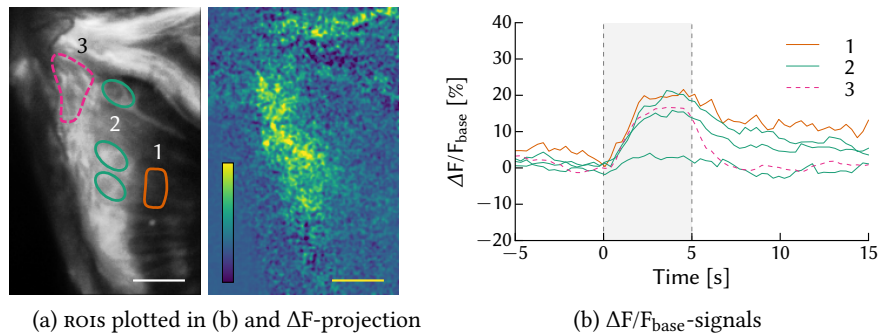


Figure 3.11: REMAINING CALCIUM SIGNALS IN *INACTIVE* MUTANTS, II (a, left) In one of the measured flies weak calcium signals were detected in proximal parts of dendrites (1), some of the corresponding cell bodies (2) and axon bundles (3). (a, right) Average of last five stimulus frames of  $\Delta F$ -data,  $\Delta F$  calibration bar: -900–2100 [a.u.], scalebar=10  $\mu\text{m}$ . (b)  $\Delta F/F_{\text{base}}$ -timetraces of dendritic, axonal and cell body ROIs. Stimulus amplitude:  $\pm 8 \mu\text{m}$ , fly genotype: *iav<sup>1</sup>* ; *n-syb-LexA::p65/+* ; *lexAop-GCaMP6m/+* ( $\sigma$ )

reached a maximum relative fluorescence increase of 20 %, more than 10 times smaller than signals usually observed in proximal dendritic regions of control flies.

### 3.5.2 Cell body- and axonal signals in inactive mutants

Besides the remaining calcium signals at the dendrites of a few JO neurons, small signals were also detected at some cell bodies and axon bundles of three flies (one example: Fig. 3.11). All signals only reached maximum relative fluorescence values below 30 % and were only visible at large sine amplitudes above  $\pm 8 \mu\text{m}$ .

In all subcellular compartments, the measured calcium increase was slower compared to control flies, with an especially strong effect at the dendrite's tips in Fig. 3.10, where the signals do not reach a plateau level anymore.

Despite the strong signal amplitude reduction compared to control flies and the somewhat changed signal time courses, *inactive* mutants clearly keep reacting to mechanical stimuli, ruling out the conclusion that Inactive is the only mechanosensitive element in the neurons of the JO. Whether this is also the case for only the sound-sensitive neurons can not be concluded from these whole-JO imaging experiments.

## 3.6 *NOMPC* MUTANTS

The TRP-channel NompC is one of the proposed members of the transduction machinery in sound-sensitive neurons of the JO, but the conclusions about its particular role are controversial in current studies. To probe its influence on individual receptor unit responses, stimulus-response curves were measured from homozygous *nompC<sup>3</sup>*-mutant flies.

### 3.6.1 *Response of all JO neurons in *nompC* mutants*

Initially, GCaMP6m was expressed in the whole JO of *nompC<sup>3</sup>/nompC<sup>3</sup>* homozygous flies via the NP0761-GAL4 driver line. In all three successfully measured flies receptor units still responded to sinusoidal arista displacement, even though mostly with very low sensitivity and response onset deflections above +/-500 nm (Fig. 3.12).

As former studies showed that a *nompC*-mutation did not alter the response of the subgroup C- and E-neurons and antennal nerve field potentials are still measurable in these flies, remaining calcium signals are consistent with the current data on the general influence of NompC. There were no receptor units visible in the analyzed optical slices which did not respond to stimulation anymore, as they were observed by Effertz et al., 2011 with widefield-calcium imaging (The receptor units corresponding to the lower traces in Fig. 3.12a, c, e, still respond to high-amplitude stimulation, but with very low amplitudes). These results thus rather resemble the GFN-whole cell voltage clamp recordings performed by Lehnert et al., 2013, in which the putative sound-sensitive JO cells of *nompC*-mutants still responded to sound stimuli, although with lower sensitivity than those of wildtype flies.

Because of the JO-wide GCaMP expression in this experiment, the visible receptor units could not be assigned to specific subgroups of the JO neurons. Therefore, one reason for the lack of non-responding receptor units could be the choice of the optical slices, which might not contain any of the neurons influenced by the *nompC*-mutation. This seems unlikely, since the ca. 145 NompC-dependent A/B-neurons account for about 30% of the whole JO (Kamikouchi et al., 2006), and the imaging plane was chosen similar to the JO15-mCherry labeling experiments in 3.4.3, where usually cells from several subgroups were visible. Another reason could be the larger displacement range used compared to the experiments of Effertz et al. If the *nompC*-impaired sound-sensitive cells correspond to the lower traces in 3.12, their small responses might have simply not been evoked at the stimulus intensities used by Effertz et al.

If the *nompC* mutation influences only a subset of the JO neurons, this might have been visible in a cluster analysis of the receptor unit responses. With the employed potentially unsuited clustering method though, little conclusions can be drawn from the fits. In contrast to the data shown in sections 3.4.2 and 3.4.3, after correction of the data at least a sensitive and an insensitive group are separated (Fig. 3.13b, f).

### 3.6.2 *Response of A/B neurons in *nompC* mutants*

To rule out the possibility that the A/B-units were overlooked in the *nompC* mutants with JO-wide GCaMP expression, the imaging experiments were repeated with flies expressing GCaMP6m only in most cells of the A/B-subgroups via JO15-GAL4 (similar to the imaging experiments performed by Effertz et al., 2011). If the *nompC* mutation indeed reduces the A/B-receptor unit response rather than completely abolishing it, calcium signals should also be

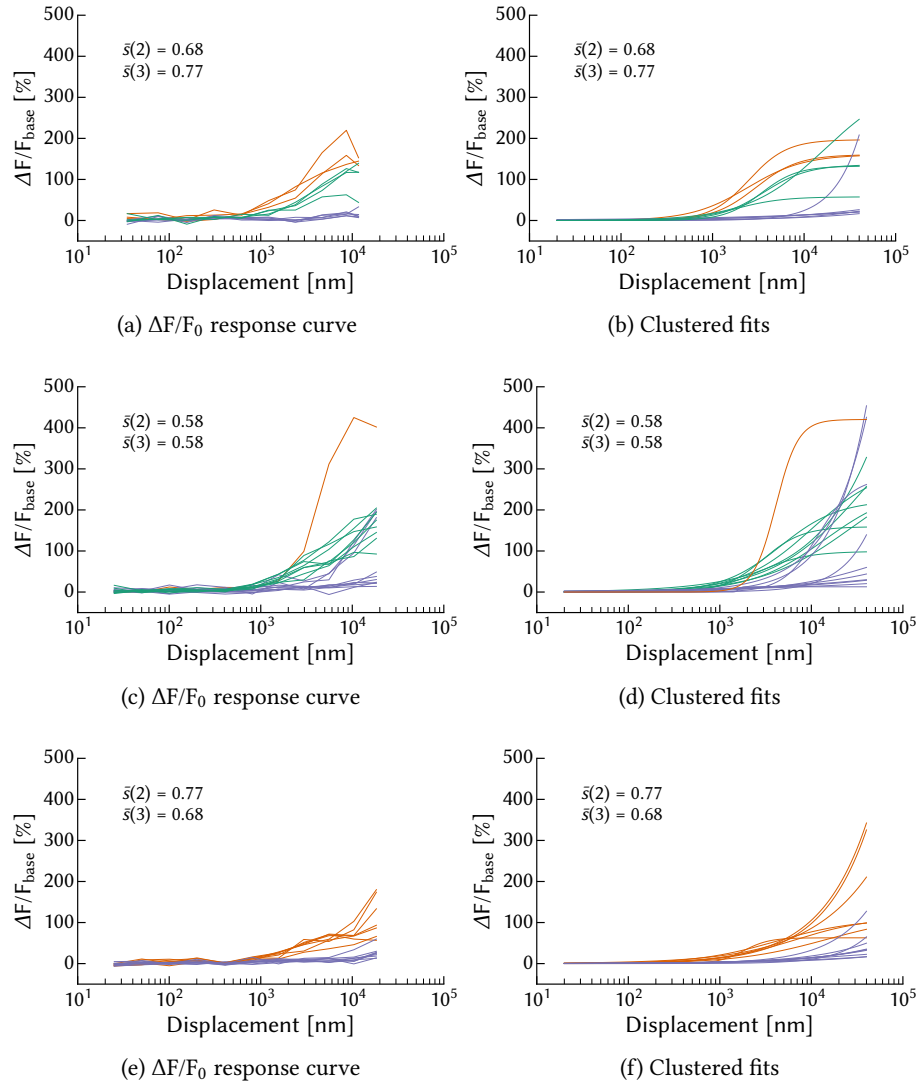


Figure 3.12: CLUSTER ANALYSIS OF JO NEURONS IN *NOMPC<sup>3</sup>/NOMPC<sup>3</sup>* FLIES (a, c, e): Stimulus-response curves of three *nompC<sup>3</sup>*-mutant flies (b, d, f): Corresponding fits with a four parameter logistic equation. Trace colors: Groups deduced from k-means cluster analysis. Fly genotypes: *w<sup>1118</sup>*; *nompC<sup>3</sup>/nompC<sup>3</sup>*; *NP0761-GAL4/UAS-GCaMP6m*

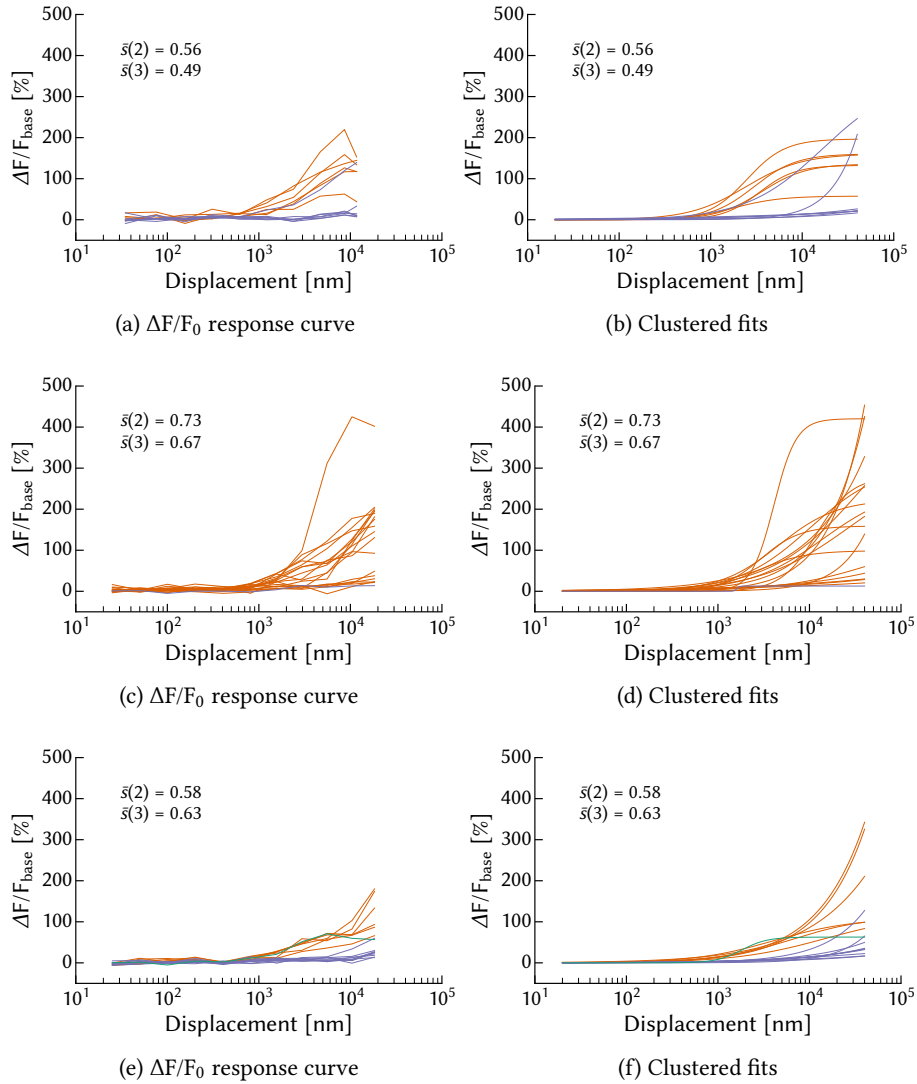


Figure 3.13: CLUSTER ANALYSIS OF JO NEURONS IN *NOMPC*<sup>3</sup>/*NOMPC*<sup>3</sup> FLIES AFTER WHITENING TRANSFORMATION (a, c, e): Stimulus-response curves of *three* *nompC*<sup>3</sup>-mutant flies (b, d, f): Corresponding fits with a four parameter logistic equation. Trace colors: Groups deduced from k-means cluster analysis after whitening transformation. Fly genotypes: *w*<sup>1118</sup>; *nompC*<sup>3</sup>/*nompC*<sup>3</sup>; *NP0761-GAL4/UAS-GCaMP6m*

detectable in these flies. A combination of two different *nompC* alleles was used in the experiments (*nompC*<sup>3</sup> and *nompC*<sup>1</sup>), as the homozygous *nompC*<sup>3</sup> flies used in 3.6.1 were not viable with the JO15-GAL4 and UAS-GCaMP6m constructs. This transheterozygous combination of *nompC*<sup>3</sup> and *nompC*<sup>1</sup> was also used by Lehnert et al., 2013 and led to the same hearing phenotypes as *nompC*<sup>3</sup>/*nompC*<sup>3</sup>.

The resulting data from four successfully measured flies shows several unexpected receptor unit responses (Fig. 3.14, 3.15). At high sine amplitudes (>+/-8  $\mu$ m), some receptor units still show calcium responses upon stimulation, yet with strongly reduced amplitudes compared to wildtype flies, supporting the data of Lehnert et al., 2013 and the results described in 3.6.1. A few units show no calcium signals anymore, which in turn would be consistent with Effertz et al., 2011. A third group of receptor units though displays a completely changed response to sound stimulation. Instead of an increase of the cytosolic calcium concentration and thus stronger fluorescence, these cells react to sinusoidal stimulation with a fluorescence decrease (Fig. 3.14d, Fig. 3.15). The decrease is dependent on stimulus strength and occurs in all measured optical slices. In comparison to the remaining increasing signals, the apparent calcium decrease happens much slower and reaches no plateau value, regardless of the subcellular compartment. This effect occurred in all four measured animals and was most prominent in axonal regions, but was neither observed by Effertz et al., 2011 nor Lehnert et al., 2013.



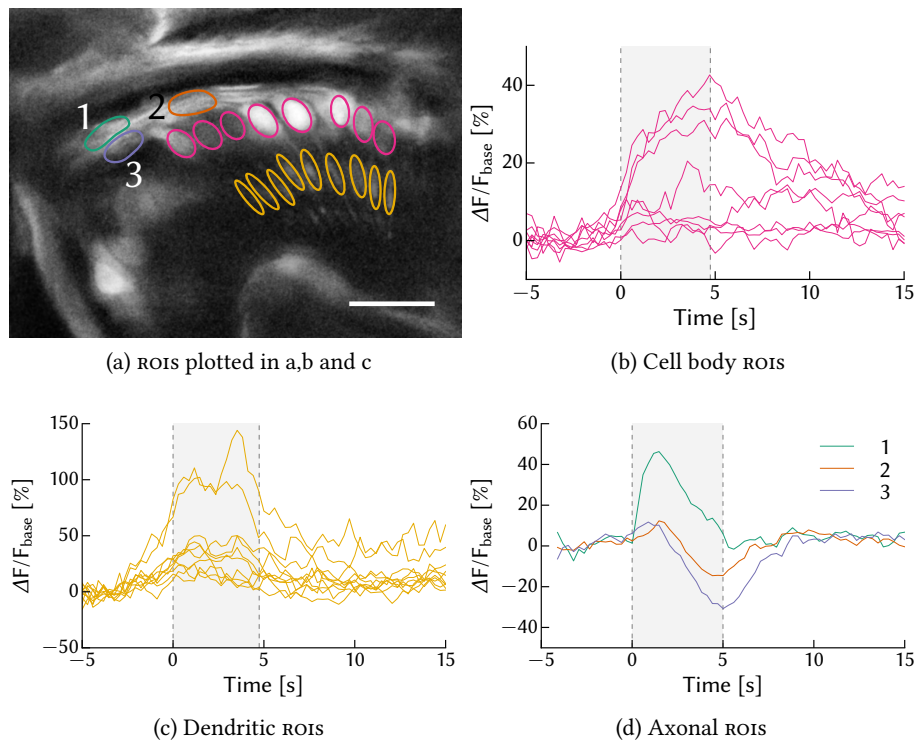


Figure 3.14: CALCIUM SIGNALS IN A/B NEURONS OF *NOMPC*<sup>3</sup>/*NOMPC*<sup>1</sup> FLIES, I. Whereas cell bodies and dendrites respond weakly or not at all to sine stimulation at  $\pm 10 \mu\text{m}$  (b,d) in this *nompC* mutant fly, in some axonal regions (d 2,3) the signal decreases by up to -35%. Scalebar:  $20 \mu\text{m}$ , example fly genotype: *w*<sup>1118</sup>; *nompC*<sup>3</sup>/*nompC*<sup>1</sup>; *JO15-GAL4/UAS-GCaMP6m*

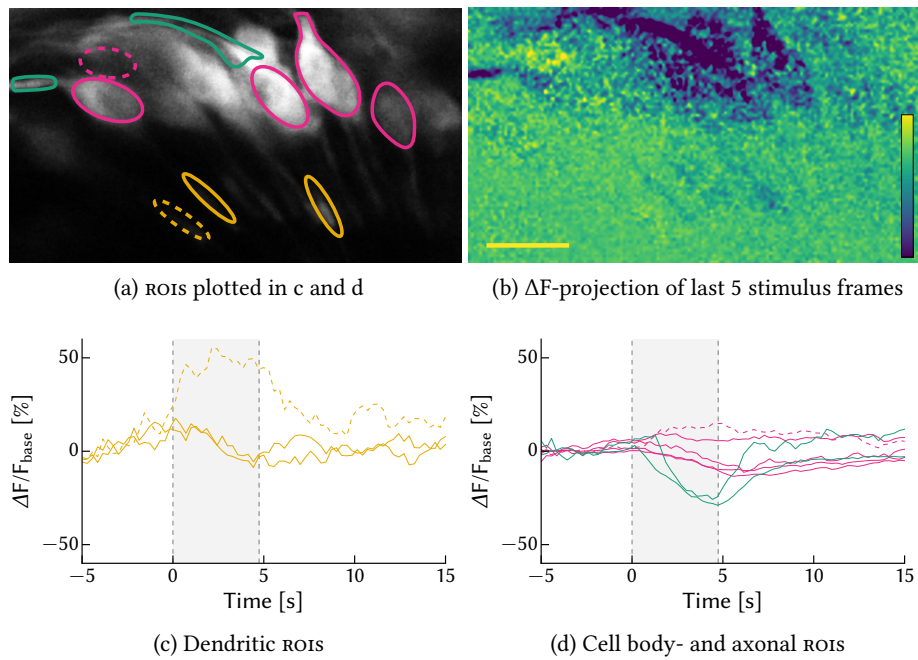


Figure 3.15: CALCIUM SIGNALS IN A/B NEURONS OF *NOMPC<sup>3</sup>/NOMPC<sup>1</sup>* FLIES, II  
 In a second *nompC* mutant fly, also some dendrites and cell bodies respond with a signal decrease to a sine stimulation of  $\pm 9 \mu\text{m}$ . Again, the signal decrease is largest in axons of receptor units. Scalebar:  $10 \mu\text{m}$ ,  $\Delta F$  calibration bar:  $-1500-500$  [a.u.], fly genotype: *w<sup>1118</sup>; nompC<sup>3</sup>/nompC<sup>1</sup>; jO15-GAL4/UAS-GCaMP6m*

DISCUSSION

---

## 4.1 TWO-PHOTON CALCIUM IMAGING IN THE JOHNSTON'S ORGAN

The calcium imaging method I established during this thesis project allows the separation of individual JO receptor unit response profiles, whereas former methods had to resort to summed responses of large JO subgroups. The method though has several limits, the most prominent one being the spatial resolution. Bound to the diffraction limit, at the used excitation wavelength the maximum theoretical resolution is around 500 nm, making complete separation of individual sensory neurons within scolopidia impossible.

The resolution is further reduced by the suboptimal light path, which includes several optical media with different refractive indices and absorption properties (water, glass, glycerol, cuticle, hemolymph, trachea and support cells). The resulting scattering and wavefront distortion enlargens the system's point spread function, reducing the two-photon excitation efficiency due to the lower photon density at its center (Chaigneau et al., 2011). This has to be counteracted with the use of higher laser powers, leading to stronger heating of the sample. The x/y-resolution is thus rather in the range of a few micrometers, and even worse in the z-axis, which is especially apparent in the cell body regions of the JO: Cell bodies of several sensory neurons appear as a maximum projection, making it impossible to properly distinguish receptor units in these regions.

The scattering and wavefront distortion also limit the imaging depth to the upper two thirds of the JO, which corresponds to about 80  $\mu\text{m}$  inside the antenna, far below the 500  $\mu\text{m}$ –1500  $\mu\text{m}$  achieved in mouse brain imaging experiments (Theer et al., 2006).

Another problem of the experimental approach is posed by the laser used for two-photon excitation. The cuticle of the fly's antenna strongly absorbs the near-infrared light, which heats up the sample to an extent that burn marks appear on the pedicel's surface and air bubbles begin to form in the Glycerol, completely preventing two-photon excitation. The duration of individual measurements thus had to be limited to a maximum of two minutes, which in combination with the slow decay time of the GCaMP signal restricted continuous measurements to three to four stimulus repetitions.

A possible way to improve the optical resolution and the excitation efficiency would be the use of adaptive optics to adjust for the inhomogeneous refractive indices as described by Wang et al., 2014, though as the distinction of the sensory neurons in one scolopidium still would be diffraction-limited, the tremendous technical effort is probably not worthwhile.

In the longer term, a promising method could be two-step fluorescence microscopy, which provides two-photon-like optical sectioning at much lower

excitation light intensities (Ingaramo et al., 2015). Currently, there are though no two-step excitable calcium sensors available.

## 4.2 SINGLE RECEPTOR UNIT RESPONSES

Despite its technical limitations, the method is capable of resolving the response of many individual JO receptor units simultaneously, providing information about the JO's activity with so far unmatched spatial resolution. Applying a series of different sine stimulus intensities reveals a broad variety of response sensitivities, very similar to the diversity in first-order auditory interneurons in the *Drosophila* brain described by Baker, 2015. This diversity by far exceeds the broad subgroups identified by Kamikouchi et al., 2009 and Matsuo et al., 2014, even though the separation into strongly sound-sensitive neurons and a second group of neurons with very small responses to sound stimuli is still reflected.

In none of the measured flies a signal drop at high stimulus intensities was observed, as it is usually visible in antennal nerve field potential recordings (the signal drops at the highest intensity shown in Fig. 3.8a and 3.9a are due to focus drift), and only few receptor units reached a response plateau level.

This similarity to the generator currents recordings by Lehnert et al., 2013 can most likely be explained by the source of the measured calcium signal. Calcium influx into the dendrites of the receptor units is believed to be a mixture of calcium entering mechanically gated transduction channels and additional influx through cation channels along the dendrite. As action potential generation putatively first happens at the cell bodies, the dendritic calcium signals essentially should reflect the graded potential of the proposed generator currents, regardless of them being elicited by ion influx via mechanically gated channels alone or also additional ion influx happening along the dendrites. Therefore, the similarity of the calcium signal response curves to the generator current dynamics seems to be a reasonable, and the lack of a response plateau in most curves can possibly be attributed to the stimulus range not exceeding the whole response range of the receptor units. These observations support the conclusion of Lehnert et al., 2013, that the saturation and decline of antennal nerve field potential recordings is due to a spike rate limit and desynchronization of receptor units, rather than to the response limit of the transduction machinery.

### 4.2.1 Fits and cluster analysis

From the subgroup-ablating experiments done by Kamikouchi et al., 2009 it was suspected, that the individual response curves recorded via calcium imaging could be reassigned to three clusters: The highly sound-sensitive, amplifying group A neurons, the less sensitive sound-preferring group B neurons and the gravity/wind receptor units of the C/E groups.

To obtain parameters usable for k-means clustering, fits of the data to a 4-parameter logistic curve were created. From uncorrected data, only in one

fly the suspected three clusters were detected as the higher scoring result compared to a two-cluster solution (Fig. 3.5c and 3.5d).

After correcting for the non-circular clusters via a whitening transformation (Fig. 3.6), in none of the flies three meaningful clusters were detected anymore. Similar clustering results were obtained from the A/B-mCherry flies, where in uncorrected data three clusters could be separated in three animals (Fig. 3.8), but only hardly two after whitening transformation of the data (Fig. 3.9).

While it is of course quite possible that there actually are no separable response clusters besides units reacting strong and very little to sound, also the clustering method used is not the best choice for the data at hand: Whereas 2D k-means clustering expects circular clusters of equal size and variance, the suspected clusters were of different size (different number of units), different variance (sound-sensitive units spread over a broader range) and of ellipsoid shape. A more appropriate clustering method such as CURE thus might lead to different analysis results (Guha et al., 2001).

#### 4.3 INFLUENCE OF THE *INACTIVE* MUTATION

As in the widefield-imaging experiments described in Wiek, 2013, stimulus-induced calcium signals were still detected in *inactive* mutants with two-photon scanning microscopy, implying that some form of mechanotransduction is still present in the JO of these flies. Compared to the results of Wiek, 2013, the signals were scarce and could not be observed in all measured flies. This difference might be resulting from the applied imaging methods. The ability of the two-photon scanning microscope to localize signals within micrometer voxels comes at the cost of potentially overlooking activity in regions not scanned during the experiment. In addition, the higher light sensitivity of the widefield system and the high-affinity calcium sensor used by Wiek, 2013 (Cameleon 2.1) allowed the detection of calcium signals which would not exceed the noise level of the two-photon scanning system. From the widefield imaging data though it can not be concluded whether the remaining signal in *inactive* null mutants measured by Wiek, 2013 arose from only a few JO cells, or from all of them. The sparse response measured with two-photon imaging therefore might either be due to a few signals managing to exceed the background noise, or an actual restriction of remaining activity to very few receptor units, leading to quite different interpretations of the role of Inactive in the JO.

In both cases the experimental results clearly show that Inactive cannot be the only mechanosensitive channel in the JO. This obviously contradicts the conclusions drawn by Lehnert et al., (2013), who propose Inactive as the sole mechanosensitive channel of the JO. Since their conclusion generalizes the results of their A/B-subgroup recordings to the whole JO, it might still be correct if restricted to these subgroups and would support the interpretation of the sparse two-photon calcium imaging signals as remnant mechanosensitivity in C/D/E-neurons.

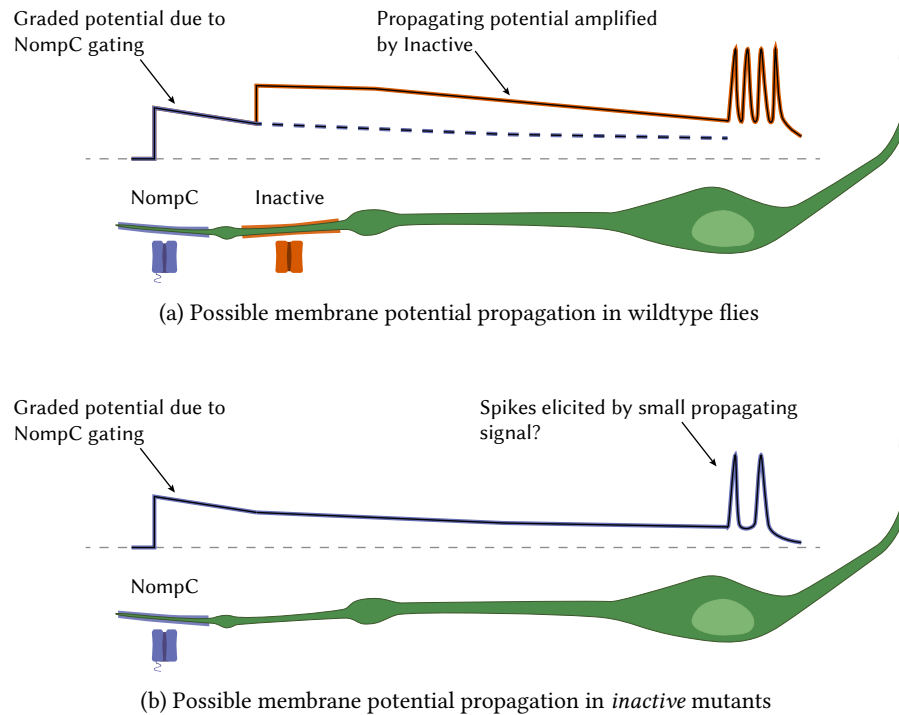


Figure 4.1: INFLUENCE OF INACTIVE ON MEMBRANE POTENTIAL PROPAGATION (a) In a model considering NompC as the primary mechanosensitive cation channel and Inactive as an element facilitating membrane potential propagation along the dendrite, the few NompC channels of sound-sensitive neurons would gate a small inward cation current, and the resulting membrane potential would be sustained along the dendrite by additional cation influx via Inactive and Nanchung. (b) In flies lacking Inactive/Nanchung, the now passively propagating membrane potential induced by the gating of NompC might still reach the cell body, assuming a sufficiently large initial amplitude.

The localization and amplitudes of the measured calcium signals support the hypothesis that Inactive is involved in boosting the transduction of mechanically evoked currents along the dendrite (Göpfert et al., 2006): Whereas in Fig. 3.10 some receptor units still show a GCaMP signal at the tips of their dendrites, it does not seem to propagate towards the cell bodies and axons of these cells. This seems to separate the dendritic signals in control flies into two parts: A primary calcium influx at the tips of the dendrites via a mechanosensitive cation channel (with NompC being a candidate for this channel), and an additional secondary influx of calcium along the proximal parts of the dendrites which is missing in *inactive* mutants (Fig. 4.1a).

In some cases though, a signal obviously is propagated along the dendrites, as seen in Fig. 3.11. As the applied stimuli in these experiments were quite large, the resulting transduction currents were maybe sufficient to reach cell bodies and axons without additional amplification via Inactive (Fig. 4.1b). Comparing the signal amplitudes in the axonal regions to control flies puts them in a range where in control flies antennal nerve potentials are easily measurable and therefore should elicit action potentials. Whether this is the

case in *inactive* mutants though can not be deduced from the slow calcium imaging, but since Inactive only localizes to the dendrites of the JO neurons, it seems unlikely that its mutation impairs axonal signal transport.

Another problem for clarifying the role of Inactive in the *Drosophila* auditory system is the controversy about its mode of activation: Whereas Kim et al., 2003 and Gong et al., 2004 were able to induce cation influx into chinese hamster ovary cells transfected with Nanchung/Inactive by applying hypoosmotic stress, Nesterov et al., 2015 were not able to reproduce these results. Inactive activation also showed only low voltage dependence, which would be necessary for direct activation by a membrane potential created by a different transduction channel. Since second messenger cascades would be too slow to allow activation phase-locking to sound stimuli of up to 500 Hz, channel activation via calcium binding could be another possible mechanism. Considering the distance between the expression sites of NompC and Inactive, calcium diffusion though also might be too slow to activate Inactive fast enough for phase locked signal amplification (Clapham, 2007).

A suitable experiment to further probe whether Inactive really alters signal propagation in the JO dendrites would be the use of Genetically Encoded Voltage Indicator (GEVI) instead of calcium sensors. As the calcium increase in the receptor units is rather a byproduct of the stimulus-evoked membrane potential change, voltage sensors would provide a much more direct measure of the transduction processes. I performed preliminary experiments with the GEVI ArcLight (Jin et al., 2012) expressed in the whole JO of non-mutant flies, and while it is possible to detect stimulus-induced signals with two-photon scanning microscopy, the achieved signal to noise ratio would not have been sufficient to reveal remaining graded potentials in mutant flies. Improved GEVIs with better signal to noise ratios and more efficient two-photon excitability though might be able to resolve the influence of Inactive on the membrane potential of JO neurons.

#### 4.4 INFLUENCE OF THE *NOMPC* MUTATION

##### 4.4.1 *nompC*<sup>3</sup>, all JO neurons

When signals from all JO neurons were measured by expressing UAS-GCaMP under control of the NP0761-GAL4 line, the *nompC* mutation reduced the maximum response amplitudes observed. This overall result is consistent with all former studies, where the *nompC* mutation reduced the amplitude of compound action potentials at the antennal nerve (Eberl et al., 2000), the amplitude of currents at the GFN (Lehnert et al., 2013) and the amplitude of calcium imaging signals in the JO (Effertz et al., 2011). Analyzing the response of individual receptor units in these flies though seems to be inconsistent with the subgroup-experiments performed by Effertz et al., 2011, as in contrast to the complete lack of sound-induced calcium signals in their experiments, no units were observed which did not produce any remaining calcium signals at all. These results thus much more resemble the findings of Lehnert et al., 2013, who observed an amplitude reduction of currents emanating from the

sound-sensitive A/B-neurons instead of an absence of transduction events. Their results though rely on the assumption, that the GFN solely receives input from the A/B-subgroups of the JO, which seems to be justified considering their morphological analysis of the axonal branches of JO neurons. As the experiments of Mu et al., 2014 though indicate additional input into the GFN from subgroup E neurons, the possibility arises that the remaining signals in the GFN of *nompC* mutants rather stem from these wind- and gravity sensing receptor units, which also in wildtype flies show lower responses to sound stimuli than the A/B cells. As the calcium imaging experiments of Effertz et al., 2011 also show signals in the C/E-neurons of *nompC*-mutants, a misconception about the GFN input could bring the results of both studies back into accordance.

#### 4.4.2 *nompC*<sup>3</sup>/*nompC*<sup>1</sup>, A/B neurons

In Kamikouchi et al., 2009, ablating all A/B-neurons reduced the sound sensitivity of the JO, leading to a rightward shift of stimulus-compound action potential response curves. Ablating subgroup B neurons alone did not lead to a response shift towards higher sound intensities, indicating that group A neurons provide most of the active sound amplification of the JO. Considering that *nompC* mutants lack active amplification but still respond to high intensity sound stimuli, it seems possible to assume that group A neurons depend on the presence of NompC in a different way than group B neurons.

This could either imply that NompC only facilitates active arista motion amplification via group A neurons and acts as part of the transduction machinery in both A and B neurons, or that it only acts as transduction channel in the most sound-sensitive group A units. As Effertz et al., 2011 and Effertz et al., 2012 found no calcium signals in group A and B neurons as well as impaired channel gating in both groups of *nompC* mutants, the first possibility with NompC as part of the transduction machinery in both groups seems more likely. Therefore, expected results of expressing GCaMP only in most of the A/B-neurons in a *nompC* mutant background were either a complete loss of sound response in all labeled units, or only a part of them.

At high stimulus intensities, the complete loss of response as well as responses with strongly reduced sensitivity were observed, indicating that at least some of the A/B neurons kept a degree of mechanosensitivity in the absence of NompC. In addition to these expected results, a stimulus-coupled negative fluorescence signal was observed in some of the labeled neurons. The signals had a different time course than signals recorded in control flies, with a slowly decreasing fluorescence (Fig. 3.14d and 3.15d), whereas the small increasing calcium signals visible in other units were more similar to the step-like signals usually observed in similar dendritic regions of control flies.

The negative GCaMP signal in some of the JO15-GAL4 labeled neurons could either be directly induced by the lack of NompC, or could resemble a process which is also active in wildtype flies, but only unmasked in sensory neurons lacking the calcium influx via NompC. If the source was an actual



calcium outflux of the neurons, this would be an unusual consequence of the lack of a channel, since it would require active outward transport of calcium from the neurons. Instead of calcium outflux induced by mechanosensitive gating in these units, the negative signal could also reflect an inhibition of the cells by surrounding mechanosensory elements, somewhat similar to the efferent feedback on vertebrate hair cells (Cooper et al., 2006). So far though, no efferent synapses were found in the JO which could contribute this inhibition and blocking of synaptic transmission in the whole nervous system of *Drosophila* did not impair active amplification in the JO (Kamikouchi, Albert, et al., 2010).

To track down the source of the observed negative calcium signals, just as for further Inactive-experiments, the availability of better genetically expressible voltage sensors would be desirable, especially since calcium imaging does not necessarily allow inference about the membrane potential of neurons, as recently investigated in the visual system of *Drosophila* (Yang et al., 2016). The voltage sensors developed in this study are also promising candidates for application in the JO).

#### 4.5 OUTLOOK

Following up on the work of Effertz et al., 2011; Kamikouchi et al., 2009 and Wiek, 2013, this study was carried out to clarify the roles of Inactive and NompC in the JO as well as characterize the function of the JO receptor units with higher resolution than previously possible.

The resulting data achieves this only partially: While recordings from single receptor units reveal a broad variety of preferred stimulus ranges, sensitivities and filter properties, they convey little information about the actual source of these properties. Whether the apparent individuality of some receptor units is based on the mechanical construction of the whole sound receiver, or if it is achieved by an equal variability in the molecular composition of the transduction machinery remains unknown. Besides further investigation of the influence of other components of the transduction machinery such as motor proteins on the receptor units' responses, closer ultrastructural analysis of the whole hearing apparatus might be beneficial.

Concerning the roles of Inactive and NompC, both major theories are to some extent supported as well as contradicted: Inactive might very well be necessary for signal propagation along the JO dendrites, and is not the only mechanosensitive channel of at least some JO neurons. Whether these neurons belong to a certain JO subgroup remains to be tested.

The *nompC* mutation decreases the overall sensitivity of the JO, but has different influences on individual A/B receptor units. Some units indeed lose all sound-induced response in the applied stimulus range, supporting Effertz et al., 2011 and NompC's role as a transduction channel candidate. Other units in the A/B groups though still remain mechanosensitive, at least limiting NompC's role to being one of several mechanosensitive channels in these neurons. The negative signals observed in *nompC* mutants at last represent a so far overlooked process of unknown origin.

As mentioned before, a tremendous improvement on the method employed in this study would be the use of voltage- instead of calcium sensors to analyze the response of the JO receptor units, which would overcome the dangerous step of comparing the information of a partially secondary signal like the intracellular calcium concentration to a primary one as actual membrane potentials recorded with electrophysiological methods.

## BIBLIOGRAPHY

---

- Akaike, H. (1974). "A new look at the statistical model identification." In: *IEEE Transactions on Automatic Control* 19.6, pp. 716–723. doi: 10.1109/TAC.1974.1100705 (cit. on p. 23).
- Akitake, Bradley, Qiuting Ren, Nina Boiko, Jinfei Ni, Takaaki Sokabe, James D Stockand, Benjamin A Eaton, and Craig Montell (2015). "Coordination and fine motor control depend on *Drosophila* TRP $\gamma$ ." In: *Nature communications* 6, p. 7288. doi: 10.1038/ncomms8288 (cit. on p. 1).
- Albert, Jörg T, Björn Nadrowski, and Martin C Göpfert (2007). "Mechanical signatures of transducer gating in the *Drosophila* ear." In: *Current biology : CB* 17.11, pp. 1000–6. doi: 10.1016/j.cub.2007.05.004 (cit. on pp. 4, 12, 21).
- Arnadóttir, Jóhanna and Martin Chalfie (2010). "Eukaryotic mechanosensitive channels." In: *Annual review of biophysics* 39, pp. 111–37. doi: 10.1146/annurev.biophys.37.032807.125836 (cit. on p. 6).
- Baker, Allison Eva (2015). "Encoding and Decoding Mechanosensory Information on Multiple Timescales." PhD thesis (cit. on pp. 26, 42).
- Ben-Arie, N, BA Hassan, NA Bermingham, DM Malicki, D Armstrong, M Matzuk, HJ Bellen, and HY Zoghbi (2000). "Functional conservation of atonal and Math1 in the CNS and PNS." In: *Development* 127.5, pp. 1039–1048 (cit. on p. 1).
- Bennet-Clark, H. C. (1971). "Acoustics of Insect Song." In: *Nature* 234.5327, pp. 255–259. doi: 10.1038/234255a0 (cit. on p. 2).
- Blount, Paul and Paul C Moe (1999). "Bacterial mechanosensitive channels: integrating physiology, structure and function." In: *Trends in Microbiology* 7.10, pp. 420–424. doi: 10.1016/S0966-842X(99)01594-2 (cit. on p. 1).
- Booth, Ian R., Michelle D. Edwards, Susan Black, Ulrike Schumann, and Samantha Miller (2007). "Mechanosensitive channels in bacteria: signs of closure?" In: *Nature Reviews Microbiology* 5.6, pp. 431–440 (cit. on p. 1).
- Brand, A H and N Perrimon (1993). "Targeted gene expression as a means of altering cell fates and generating dominant phenotypes." In: *Development (Cambridge, England)* 118.2, pp. 401–15 (cit. on p. 11).
- Chadha, Abhishek, Maki Kaneko, and Boaz Cook (2015). "NOMPC-dependent mechanotransduction shapes the dendrite of proprioceptive neurons." In: *Neuroscience letters* 597, pp. 111–6. doi: 10.1016/j.neulet.2015.04.033 (cit. on p. 6).
- Chaigneau, Emmanuelle, Amanda J Wright, Simon P Poland, John M Girkin, and R Angus Silver (2011). "Impact of wavefront distortion and scattering on 2-photon microscopy in mammalian brain tissue." In: *Optics express* 19.23, pp. 22755–74. doi: 10.1364/OE.19.022755 (cit. on p. 41).
- Chen, Tsai-Wen, Trevor J Wardill, Yi Sun, Stefan R Pulver, Sabine L Renninger, Amy Baohan, Eric R Schreiter, Rex a Kerr, Michael B Orger, Vivek Jayara-

- man, Loren L Looger, Karel Svoboda, and Douglas S Kim (2013). "Ultrasensitive fluorescent proteins for imaging neuronal activity." In: *Nature* 499.7458, pp. 295–300. doi: 10.1038/nature12354 (cit. on p. 11).
- Clapham, David E (2007). "Calcium signaling." In: *Cell* 131.6, pp. 1047–58. doi: 10.1016/j.cell.2007.11.028 (cit. on p. 45).
- Cooper, N P and J J Guinan (2006). "Efferent-mediated control of basilar membrane motion." In: *The Journal of physiology* 576.Pt 1, pp. 49–54. doi: 10.1113/jphysiol.2006.114991 (cit. on p. 47).
- Davis, Hallowell (1983). "An active process in cochlear mechanics." In: *Hearing Research* 9.1, pp. 79–90. doi: 10.1016/0378-5955(83)90136-3 (cit. on p. 4).
- Denk, W, J. Strickler, and W. Webb (1990). "Two-photon laser scanning fluorescence microscopy." In: *Science* 248.4951, pp. 73–76. doi: 10.1126/science.2321027 (cit. on p. 8).
- Dubin, Adrienne E. et al. (2010). "Nociceptors: the sensors of the pain pathway." In: *Journal of Clinical Investigation* 120.11, pp. 3760–3772. doi: 10.1172/JCI42843 (cit. on p. 1).
- Eberl, Daniel F., Robert W. Hardy, and Maurice J. Kernan (2000). "Genetically Similar Transduction Mechanisms for Touch and Hearing in *Drosophila*." In: *J. Neurosci.* 20.16, pp. 5981–5988 (cit. on pp. 2, 4, 6, 7, 45).
- Effertz, Thomas, Björn Nadrowski, David Piepenbrock, Jörg T Albert, and Martin C Göpfert (2012). "Direct gating and mechanical integrity of *Drosophila* auditory transducers require TRPN1." In: *Nature neuroscience* 15.9, pp. 1198–200. doi: 10.1038/nn.3175 (cit. on pp. 5–7, 46).
- Effertz, Thomas, Robert Wiek, and Martin C Göpfert (2011). "NompC TRP channel is essential for *Drosophila* sound receptor function." In: *Current biology : CB* 21.7, pp. 592–7. doi: 10.1016/j.cub.2011.02.048 (cit. on pp. 4, 6, 19, 25, 26, 35, 38, 45–47).
- Ewing, Arthur W. (1978). "The antenna of *Drosophila* as a 'love song' receptor." In: *Physiological Entomology* 3.1, pp. 33–36. doi: 10.1111/j.1365-3032.1978.tb00129.x (cit. on p. 2).
- Fettiplace, Robert (2006). "Active hair bundle movements in auditory hair cells." In: *The Journal of physiology* 576.Pt 1, pp. 29–36. doi: 10.1113/jphysiol.2006.115949 (cit. on p. 4).
- Fettiplace, Robert and Kyunghye X Kim (2014). "The physiology of mechano-electrical transduction channels in hearing." In: *Physiological reviews* 94.3, pp. 951–86. doi: 10.1152/physrev.00038.2013 (cit. on p. 1).
- Geurten, Bart R H, Philipp Jähde, Kristina Corthals, and Martin C Göpfert (2014). "Saccadic body turns in walking *Drosophila*." In: *Frontiers in behavioral neuroscience* 8, p. 365. doi: 10.3389/fnbeh.2014.00365 (cit. on p. 59).
- Gong, Jiaxin, Qingxiu Wang, and Zuoren Wang (2013). "NOMPC is likely a key component of *Drosophila* mechanotransduction channels." In: *The European journal of neuroscience* 38.1, pp. 2057–64. doi: 10.1111/ejn.12214 (cit. on p. 6).
- Gong, Zhefeng, Wonseok Son, Yun Doo Chung, Janghwan Kim, Dong Wook Shin, Colleen a McClung, Yong Lee, Hye Won Lee, Deok-Jin Chang, Bong-

- Kiun Kaang, Hawon Cho, Uhtaek Oh, Jay Hirsh, Maurice J Kernan, and Changsoo Kim (2004). “Two interdependent TRPV channel subunits, inactive and Nanchung, mediate hearing in *Drosophila*.” In: *The Journal of neuroscience : the official journal of the Society for Neuroscience* 24.41, pp. 9059–66. DOI: 10 . 1523 / JNEUROSCI . 1645 - 04 . 2004 (cit. on pp. 4, 5, 45).
- Göpfert, M C, a D L Humphris, J T Albert, D Robert, and O Hendrich (2005). “Power gain exhibited by motile mechanosensory neurons in *Drosophila* ears.” In: *Proceedings of the National Academy of Sciences of the United States of America* 102.2, pp. 325–30. DOI: 10 . 1073 / pnas . 0405741102 (cit. on p. 4).
- Göpfert, M C and D Robert (2003). “Motion generation by *Drosophila* mechanosensory neurons.” In: *Proceedings of the National Academy of Sciences of the United States of America* 100.9, pp. 5514–9. DOI: 10 . 1073 / pnas . 0737564100 (cit. on pp. 4, 14).
- Göpfert, Martin C and Daniel Robert (2002). “The mechanical basis of *Drosophila* audition.” In: *The Journal of experimental biology* 205.Pt 9, pp. 1199–208 (cit. on pp. 2, 4).
- Göpfert, MC, Jörg T Albert, B Nadrowski, and A Kamikouchi (2006). “Specification of auditory sensitivity by *Drosophila* TRP channels.” In: *Nature neuroscience* 9.8, pp. 999–1000. DOI: 10 . 1038 / nn1735 (cit. on pp. 1, 5, 7, 44).
- Gras, Heribert (2014). “A multiaxis device for in-focus manipulation of objects under a dissecting microscope.” In: *Journal of microscopy* 256.1, pp. 1–5. DOI: 10 . 1111 / jmi . 12152 (cit. on p. 12).
- Guha, Sudipto, Rajeev Rastogi, and Kyuseok Shim (2001). “Cure: an efficient clustering algorithm for large databases.” In: *Information Systems* 26.1, pp. 35–58. DOI: 10 . 1016 / S0306 - 4379 (01) 00008 - 4 (cit. on p. 43).
- Hayashi, Shigeo, Kei Ito, Yukiko Sado, Misako Taniguchi, Ai Akimoto, Hiroko Takeuchi, Toshiro Aigaki, Fumio Matsuzaki, Hideki Nakagoshi, Teiichi Tanimura, Ryu Ueda, Tadashi Uemura, Motojiro Yoshihara, and Satoshi Goto (2002). “GETDB, a database compiling expression patterns and molecular locations of a collection of gal4 enhancer traps.” In: *Genesis* 34.1-2, pp. 58–61. DOI: 10 . 1002 / gene . 10137 (cit. on p. 16).
- Homyk, T (1977). “Behavioral Mutants of *Drosophila melanogaster*. II. Behavioral Analysis and Focus Mapping.” In: *Genetics* 87.1, pp. 105–28 (cit. on p. 5).
- Howard, J. and A.J. Hudspeth (1988). “Compliance of the hair bundle associated with gating of mechano-electrical transduction channels in the Bullfrog’s saccular hair cell.” In: *Neuron* 1.3, pp. 189–199. DOI: 10 . 1016 / 0896 - 6273 (88) 90139 - 0 (cit. on p. 4).
- Hudspeth, A J (2008). “Making an effort to listen: mechanical amplification in the ear.” In: *Neuron* 59.4, pp. 530–45. DOI: 10 . 1016 / j . neuron . 2008 . 07 . 012 (cit. on p. 1).
- Ingaramo, Maria, Andrew G York, Eric J Andrade, Kristin Rainey, and George H Patterson (2015). “Two-photon-like microscopy with orders-of-magnitude

- lower illumination intensity via two-step fluorescence.” In: *Nature communications* 6, p. 8184. doi: 10 . 1038/ncomms9184 (cit. on p. 42).
- Jin, Lei, Zhou Han, Jelena Platisa, Julian R A Woollorton, Lawrence B Cohen, and Vincent A Pieribone (2012). “Single action potentials and subthreshold electrical events imaged in neurons with a fluorescent protein voltage probe.” In: *Neuron* 75.5, pp. 779–85. doi: 10 . 1016/j . neuron . 2012 . 06 . 040 (cit. on p. 45).
- Johnston, C (1855). “Auditory apparatus of the *Culex* mosquito.” In: *Quarterly Journal of Microscopical Science* III, pp. 97–102 (cit. on p. 3).
- Jonsson, Thorin, Edward A Kravitz, and Ralf Heinrich (2011). “Sound production during agonistic behavior of male *Drosophila melanogaster*.” In: *Fly* 5.1, pp. 29–38 (cit. on p. 2).
- Kamikouchi, Azusa, Jörg T Albert, and Martin C Göpfert (2010). “Mechanical feedback amplification in *Drosophila* hearing is independent of synaptic transmission.” In: *The European journal of neuroscience* 31.4, pp. 697–703. doi: 10 . 1111/j . 1460-9568 . 2010 . 07099 . x (cit. on p. 47).
- Kamikouchi, Azusa, Hidehiko K Inagaki, Thomas Effertz, Oliver Hendrich, André Fiala, Martin C Göpfert, and Kei Ito (2009). “The neural basis of *Drosophila* gravity-sensing and hearing.” In: *Nature* 458.7235, pp. 165–71. doi: 10 . 1038/nature07810 (cit. on pp. 4, 5, 19, 25, 26, 42, 46, 47).
- Kamikouchi, Azusa, Takashi Shimada, and K. Ito (2006). “Comprehensive classification of the auditory sensory projections in the brain of the fruit fly *Drosophila melanogaster*.” In: *The Journal of comparative neurology* 499.3, pp. 317–356. doi: 10 . 1002/cne (cit. on pp. 4, 6, 11, 16, 26, 35).
- Kamikouchi, Azusa, Robert Wiek, Thomas Effertz, Martin C Göpfert, and André Fiala (2010). “Transcuticular optical imaging of stimulus-evoked neural activities in the *Drosophila* peripheral nervous system.” In: *Nature protocols* 5.7, pp. 1229–35. doi: 10 . 1038/nprot . 2010 . 85 (cit. on p. 12).
- Kang, Lijun, Jingwei Gao, William R Schafer, Zhixiong Xie, and X Z Shawn Xu (2010). “*C. elegans* TRP family protein TRP-4 is a pore-forming subunit of a native mechanotransduction channel.” In: *Neuron* 67.3, pp. 381–91. doi: 10 . 1016/j . neuron . 2010 . 06 . 032 (cit. on p. 6).
- Karak, Somdatta, Julie S Jacobs, Maike Kittelmann, Christian Spalthoff, Radoslaw Katana, Elena Sivan-Loukianova, Michael A Schon, Maurice J Kernan, Daniel F Eberl, and Martin C Göpfert (2015). “Diverse Roles of Axonemal Dyneins in *Drosophila* Auditory Neuron Function and Mechanical Amplification in Hearing.” In: *Scientific reports* 5, p. 17085. doi: 10 . 1038/srep17085 (cit. on p. 4).
- Kernan, Maurice, David Cowan, and C S Zuker (1994). “Genetic dissection of mechanosensory transduction: Mechanoreception-defective mutations of *Drosophila*.” In: *Neuron* 12.6, pp. 1195–1206. doi: 10 . 1016 / 0896 - 6273 (94) 90437 - 5 (cit. on p. 5).
- Kim, Janghwan, Yun Doo Chung, Dae-Young Park, SooKyung Choi, Dong Wook Shin, Heun Soh, Hye Won Lee, Wonseok Son, Jeongbin Yim, Chul-Seung Park, Maurice J Kernan, and Changsoo Kim (2003). “A TRPV family ion channel required for hearing in *Drosophila*.” In: *Nature* 424, pp. 81–84. doi: 10 . 1038/nature01733 (cit. on pp. 5, 45).

- Lai, Sen-Lin and Tzumin Lee (2006). “Genetic mosaic with dual binary transcriptional systems in *Drosophila*.” In: *Nature neuroscience* 9.5, pp. 703–9. doi: 10.1038/nn1681 (cit. on p. 11).
- Lee, Jeongmi, Sungjin Moon, Yoonseok Cha, and Yun Doo Chung (2010). “*Drosophila* TRPN(=NOMPC) channel localizes to the distal end of mechanosensory cilia.” In: *PloS one* 5.6, e11012. doi: 10.1371/journal.pone.0011012 (cit. on pp. 5, 32).
- Lehnert, Brendan P, Allison E Baker, Quentin Gaudry, Ann-Shyn Chiang, and Rachel I Wilson (2013). “Distinct roles of TRP channels in auditory transduction and amplification in *Drosophila*.” In: *Neuron* 77.1, pp. 115–28. doi: 10.1016/j.neuron.2012.11.030 (cit. on pp. 4–6, 8, 25, 32, 35, 38, 42, 43, 45).
- Liang, Xin, Johnson Madrid, Roland Gärtner, Jean-Marc Verbavatz, Christoph Schiklenk, Michaela Wilsch-Bräuninger, Aliona Bogdanova, Florian Stenger, Axel Voigt, and Jonathon Howard (2013). “A NOMPC-dependent membrane-microtubule connector is a candidate for the gating spring in fly mechanoreceptors.” In: *Current biology : CB* 23.9, pp. 755–63. doi: 10.1016/j.cub.2013.03.065 (cit. on p. 6).
- Maksimovic, Srdjan, Masashi Nakatani, Yoshichika Baba, Aislyn M. Nelson, Kara L. Marshall, Scott A. Wellnitz, Pervez Firozi, Seung-Hyun Woo, Sanjeev Ranade, Ardem Patapoutian, and Ellen A. Lumpkin (2014). “Epidermal Merkel cells are mechanosensory cells that tune mammalian touch receptors.” In: *Nature* advance on. doi: 10.1038/nature13250 (cit. on p. 1).
- Manning, A. (1967). “Antennae and Sexual Receptivity in *Drosophila melanogaster* Females.” In: *Science* 158.3797, pp. 136–137. doi: 10.1126/science.158.3797.136 (cit. on p. 2).
- Matsuo, Eriko, Daichi Yamada, Yuki Ishikawa, Tomonori Asai, Hiroshi Ishimoto, and Azusa Kamikouchi (2014). “Identification of novel vibration- and deflection-sensitive neuronal subgroups in Johnston’s organ of the fruit fly.” In: *Frontiers in Physiology* 5. doi: 10.3389/fphys.2014.00179 (cit. on pp. 4, 42).
- Mu, Laiyong, Jonathan P Bacon, Kei Ito, and Nicholas J Strausfeld (2014). “Responses of *Drosophila* giant descending neurons to visual and mechanical stimuli.” In: *The Journal of experimental biology* 217.Pt 12, pp. 2121–9. doi: 10.1242/jeb.099135 (cit. on pp. 7, 46).
- Nadrowski, Björn, Jörg T Albert, and Martin C Göpfert (2008). “Transducer-based force generation explains active process in *Drosophila* hearing.” In: *Current biology : CB* 18.18, pp. 1365–72. doi: 10.1016/j.cub.2008.07.095 (cit. on p. 4).
- Nakai, J, M Ohkura, and K Imoto (2001). “A high signal-to-noise Ca(2+) probe composed of a single green fluorescent protein.” In: *Nature biotechnology* 19.2, pp. 137–41. doi: 10.1038/84397 (cit. on p. 11).
- Nesterov, Alexandre, Christian Spalthoff, Ramani Kandasamy, Radoslav Katanana, Nancy B. Rankl, Marta Andrés, Philipp Jähde, John A. Dorsch, Lynn F. Stam, Franz-Josef Braun, Ben Warren, Vincent L. Salgado, and Martin C. Göpfert (2015). “TRP Channels in Insect Stretch Receptors as Insecti-

- cide Targets.” In: *Neuron* 86.3, pp. 665–671. DOI: 10.1016/j.neuron.2015.04.001 (cit. on pp. 5, 45, 59).
- Newville, Matthew, Antonino Ingargiola, Till Stensitzki, and Daniel B. Allen (2014). “LMFIT: Non-Linear Least-Square Minimization and Curve-Fitting for Python.” In: DOI: 10.5281/zenodo.11813 (cit. on p. 15).
- Oldfield, B. P. and K. G. Hill (1986). “Functional organization of insect auditory sensilla.” In: *Journal of Comparative Physiology A* 158.1, pp. 27–34. DOI: 10.1007/BF00614517 (cit. on p. 3).
- Pedregosa, Fabian, Gaël Varoquaux, Alexandre Gramfort, Vincent Michel, Bertrand Thirion, Olivier Grisel, Mathieu Blondel, Peter Prettenhofer, Ron Weiss, Vincent Dubourg, Jake Vanderplas, Alexandre Passos, David Cournapeau, Matthieu Brucher, Matthieu Perrot, and Édouard Duchesnay (2012). “Scikit-learn: Machine Learning in Python.” In: *Journal of Machine Learning Research* 12, pp. 2825–2830. DOI: 10.1007/s13398-014-0173-7. 2. arXiv: 1201.0490 (cit. on p. 15).
- Rousseeuw, Peter J. (1987). “Silhouettes: A graphical aid to the interpretation and validation of cluster analysis.” In: *Journal of Computational and Applied Mathematics* 20, pp. 53–65. DOI: 10.1016/0377-0427(87)90125-7 (cit. on pp. 15, 26).
- Roy, Madhuparna, Elena Sivan-Loukianova, and Daniel F Eberl (2013). “Cell-type-specific roles of Na<sup>+</sup>/K<sup>+</sup> ATPase subunits in *Drosophila* auditory mechanosensation.” In: *Proceedings of the National Academy of Sciences of the United States of America* 110.1, pp. 181–6. DOI: 10.1073/pnas.1208866110 (cit. on p. 3).
- Schilcher, Florian von (1976). “The function of pulse song and sine song in the courtship of *Drosophila melanogaster*.” In: *Animal Behaviour* 24.3, pp. 622–625. DOI: 10.1016/S0003-3472(76)80076-0 (cit. on p. 2).
- Schindelin, Johannes, Ignacio Arganda-Carreras, Erwin Frise, Verena Kaynig, Mark Longair, Tobias Pietzsch, Stephan Preibisch, Curtis Rueden, Stephan Saalfeld, Benjamin Schmid, Jean-Yves Tinevez, Daniel James White, Volker Hartenstein, Kevin Eliceiri, Pavel Tomancak, and Albert Cardona (2012). “Fiji: an open-source platform for biological-image analysis.” In: *Nature methods* 9.7, pp. 676–82. DOI: 10.1038/nmeth.2019 (cit. on p. 14).
- Senthilan, Pingkalai R, David Piepenbrock, Guvanch Ovezmyradov, Björn Nadrowski, Susanne Bechstedt, Stephanie Pauls, Margret Winkler, Wiebke Möbius, Jonathon Howard, and Martin C Göpfert (2012). “*Drosophila* auditory organ genes and genetic hearing defects.” In: *Cell* 150.5, pp. 1042–54. DOI: 10.1016/j.cell.2012.06.043 (cit. on pp. 1, 4).
- Sharma, Yashoda, Una Cheung, Ellen W Larsen, and Daniel F Eberl (2002). “PPTGAL, a convenient Gal4 P-element vector for testing expression of enhancer fragments in *Drosophila*.” In: *Genesis (New York, N.Y. : 2000)* 34.1-2, pp. 115–8. DOI: 10.1002/gene.10127 (cit. on p. 11).
- Shearin, Harold K., Alisa R. Dvarishkis, Craig D. Kozeluh, and R. Steven Stowers (2013). “Expansion of the Gateway MultiSite Recombination Cloning Toolkit.” In: *PLoS ONE* 8.10. Ed. by Brian D. McCabe, e77724. DOI: 10.1371/journal.pone.0077724 (cit. on p. 11).



- Shearin, Harold K, Ian S Macdonald, Laura P Spector, and R Steven Stowers (2014). “Hexameric GFP and mCherry reporters for the *Drosophila* GAL4, Q, and LexA transcription systems.” In: *Genetics* 196.4, pp. 951–60. DOI: 10 . 1534/genetics . 113 . 161141 (cit. on p. 11).
- Shigekazu, Uga and M Kuwabara (1965). “On the fine structure of the chordotonal sensillum in antenna of *Drosophila melanogaster*.” In: *Journal of Electron ...* 14.3 (cit. on p. 3).
- Sidi, Samuel, Rainer W Friedrich, and Teresa Nicolson (2003). “NompC TRP channel required for vertebrate sensory hair cell mechanotransduction.” In: *Science (New York, N.Y.)* 301.5629, pp. 96–9. DOI: 10 . 1126 / science . 1084370 (cit. on p. 6).
- Storace, Douglas A, Oliver R Braubach, Lei Jin, Lawrence B Cohen, and Uhna Sung (2015). “Monitoring brain activity with protein voltage and calcium sensors.” In: *Scientific reports* 5, p. 10212. DOI: 10 . 1038 / srep10212 (cit. on p. 23).
- Sun, Yishan, Lei Liu, Yehuda Ben-Shahar, Julie S Jacobs, Daniel F Eberl, and Michael J Welsh (2009). “TRPA channels distinguish gravity sensing from hearing in Johnston’s organ.” In: *Proceedings of the National Academy of Sciences of the United States of America* 106.32, pp. 13606–11. DOI: 10 . 1073 / pnas . 0906377106 (cit. on p. 5).
- Theer, Patrick and Winfried Denk (2006). “On the fundamental imaging-depth limit in two-photon microscopy.” In: *Journal of the Optical Society of America A* 23.12, p. 3139. DOI: 10 . 1364 / JOSAA . 23 . 003139 (cit. on p. 41).
- Thévenaz, P, U E Ruttimann, and M Unser (1998). “A pyramid approach to subpixel registration based on intensity.” In: *IEEE transactions on image processing : a publication of the IEEE Signal Processing Society* 7.1, pp. 27–41. DOI: 10 . 1109 / 83 . 650848 (cit. on p. 14).
- Todi, Sokol V, Yashoda Sharma, and Daniel F Eberl (2004). “Anatomical and molecular design of the *Drosophila* antenna as a flagellar auditory organ.” In: *Microscopy research and technique* 63.6, pp. 388–99. DOI: 10 . 1002 / jemt . 20053 (cit. on p. 3).
- Tootoonian, Sina, Philip Coen, Risa Kawai, and Mala Murthy (2012). “Neural representations of courtship song in the *Drosophila* brain.” In: *The Journal of neuroscience : the official journal of the Society for Neuroscience* 32.3, pp. 787–98. DOI: 10 . 1523 / JNEUROSCI . 5104 - 11 . 2012 (cit. on p. 4).
- Walker, R. G. (2000). “A *Drosophila* Mechanosensory Transduction Channel.” In: *Science* 287.5461, pp. 2229–2234. DOI: 10 . 1126 / science . 287 . 5461 . 2229 (cit. on p. 6).
- Walt, Stéfan van der, S Chris Colbert, and Gaël Varoquaux (2011). “The NumPy Array: A Structure for Efficient Numerical Computation.” In: *Computing in Science & Engineering* 13.2, pp. 22–30. DOI: 10 . 1109 / MCSE . 2011 . 37. arXiv: 1102 . 1523 (cit. on p. 15).
- Wang, Kai, Daniel E Milkie, Ankur Saxena, Peter Engerer, Thomas Misgeld, Marianne E Bronner, Jeff Mumm, and Eric Betzig (2014). “Rapid adaptive optical recovery of optimal resolution over large volumes.” In: *Nature methods* 11.6, pp. 625–8. DOI: 10 . 1038 / nmeth . 2925 (cit. on p. 41).

- Wiek, Robert Jago (2013). "A Functional Characterisation of *Drosophila* Chordotonal Organs." PhD thesis (cit. on pp. 5, 32, 43, 47).
- Yan, Zhiqiang, Wei Zhang, Ye He, David Gorczyca, Yang Xiang, Li E Cheng, Shan Meltzer, Lily Yeh Jan, and Yuh Nung Jan (2013). "*Drosophila* NOMPC is a mechanotransduction channel subunit for gentle-touch sensation." In: *Nature* 493.7431, pp. 221–5. DOI: 10 . 1038/nature11685 (cit. on p. 6).
- Yang, Helen H., François St-Pierre, Xulu Sun, Xiaozhe Ding, Michael Z. Lin, and Thomas R. Clandinin (2016). "Subcellular Imaging of Voltage and Calcium Signals Reveals Neural Processing In Vivo." In: *Cell*. DOI: 10 . 1016/j . cell . 2016 . 05 . 031 (cit. on p. 47).
- Yorozu, Suzuko, Allan Wong, Brian J Fischer, Heiko Dankert, Maurice J Kernan, Azusa Kamikouchi, Kei Ito, and David J Anderson (2009). "Distinct sensory representations of wind and near-field sound in the *Drosophila* brain." In: *Nature* 458.7235, pp. 201–5. DOI: 10 . 1038/nature07843 (cit. on pp. 4, 25).
- Zhang, Wei, Li E Cheng, Maike Kittelmann, Jiefu Li, Maja Petkovic, Tong Cheng, Peng Jin, Zhenhao Guo, Martin C Göpfert, Lily Yeh Jan, and Yuh Nung Jan (2015). "Ankyrin Repeats Convey Force to Gate the NOMPC Mechanotransduction Channel." In: *Cell* 162.6, pp. 1391–403 (cit. on p. 6).
- Zhang, Wei, Zhiqiang Yan, Lily Yeh Jan, and Yuh Nung Jan (2013). "Sound response mediated by the TRP channels NOMPC, NANCHUNG, and INACTIVE in chordotonal organs of *Drosophila* larvae." In: *Proceedings of the National Academy of Sciences of the United States of America*. DOI: 10 . 1073/pnas . 1312477110 (cit. on p. 6).
- Zhu, Xiaoying, Roland Bouffanais, and Dick K. P. Yue (2015). "Interplay between motility and cell-substratum adhesion in amoeboid cells." In: *Biomechanics* 9.5, p. 054112. DOI: 10 . 1063/1 . 4931762 (cit. on p. 1).

## ACKNOWLEDGEMENTS

---

Nach fast fünf Jahren in der Abteilung für zelluläre Neurobiologie möchte ich hier allen danken, die mich in dieser Zeit unterstützt, begleitet und betreut haben. Zunächst meinem Doktorvater Martin Göpfert, der mir mit reichlich Geduld ermöglicht hat, diese Arbeit mit allen Freiheiten, die ich mir wünschen konnte abzuschließen. Außerdem den Mitgliedern meines Thesis committees, Prof. Dr. Siegrid Löwel und Prof. Dr. André Fiala, dass sie sich die Zeit genommen haben, meine Promotion zu begleiten.

Margret, Silvia und Steffi möchte ich für die Sicherstellung unserer Versorgung mit Fliegenfutter, Lakritz und Kuchen danken, Gudrun für ihre Geduld mit Reisekostenabrechnungen und ähnlichem. Ohne euch würde die Arbeitsgruppe vermutlich innerhalb weniger Tage zugrunde gehen.

Vielen Dank an Christian, der immer ein offenes Ohr für die Freuden des calcium imagings hatte, und mit mir zusammen ein Labor voller Wiek'scher Altlasten ertragen hat (außerdem vielen Dank für die Übernahme der Kaffeekasse während meiner Elternzeit). Bei Krissy möchte ich mich nochmals für ihre unschätzbare Unterstützung bei der Organisation des NeuroDoWo 2013 bedanken und selbstverständlich für ihre Hilfe während des Schneckrezeptorkurses. Bei beiden natürlich auch generell für eure Freund- und Gesellschaft während meiner Doktorarbeitszeit.

Heribert Gras möchte ich dafür danken, dass er mich seit dem Beginn meines Studiums immer wieder daran erinnert hat, dass Wissenschaft so sein kann, wie ich sie mir immer vorgestellt habe. Ich werde niemals die Bewunderung für die Idee verlieren, ImageJ für die Auswertung elektrophysiologischer Daten zu verwenden.

Bart, Diego, Andrea, Robert, Radek, Marta, Ralf, Andreas, Damiano, Seolhee, Natasa, Somdatta, Mit, David, Maike und Paule: Vielen Dank für Hilfe, Diskussionen, Ratschläge, Gesellschaft, Essen und Kaffeepausen.

Bei Hannahs Großeltern möchte ich mich für zahlreiche Stunden babysitting während der Endphase unserer Promotionen und die Unterstützung in den Jahren davor bedanken, ihr seid uns eine große Hilfe.

Hannah und Mona, vielen, vielen Dank, dass es euch gibt!



## CURRICULUM VITAE

---

### PERSONAL INFORMATION

NAME Philipp Jähde  
DATE OF BIRTH August 16<sup>th</sup>, 1985  
PLACE OF BIRTH Hessisch-Lichtenau  
NATIONALITY german

### EDUCATION

06/2011—PRESENT PhD student, University of Göttingen,  
Department of Cellular Neurobiology  
Thesis: “Analyzing receptor responses in the *Drosophila*  
Johnston’s organ with two-photon microscopy”  
Supervisor: Prof. Dr. Martin Göpfert

02/2010—12/2010 Diploma Thesis, University of Göttingen,  
Department of Cellular Neurobiology  
Thesis: “Richtungsverarbeitung im auditorischen  
System von *Gryllus bimaculatus*”  
Supervisor: Prof. Dr. Andreas Stumpner

2005—2010 Diploma studies in Biology  
Georg-August-University of Göttingen

### PUBLICATIONS

Alexandre Nesterov, Christian Spalthoff, Ramani Kandasamy, Radoslav Katanana, Nancy B. Rankl, Marta Andrés, Philipp Jähde, John A. Dorsch, Lynn F. Stam, Franz-Josef Braun, Ben Warren, Vincent L. Salgado, and Martin C. Göpfert (2015). “TRP Channels in Insect Stretch Receptors as Insecticide Targets.” In: *Neuron* 86.3, pp. 665–671. doi: 10 . 1016 / j . neuron . 2015 . 04 . 001

Bart R H Geurten, Philipp Jähde, Kristina Corthals, and Martin C Göpfert (2014). “Saccadic body turns in walking *Drosophila*.” In: *Frontiers in behavioral neuroscience* 8, p. 365. doi: 10 . 3389 / fnbeh . 2014 . 00365

CONFERENCE PRESENTATIONS

- 03/2015 11<sup>th</sup> Meeting of the German Neuroscience Society, Poster  
“Measuring single cell responses in the *Drosophila*  
hearing organ with two-photon microscopy”
- 03/2013 10<sup>th</sup> Meeting of the German Neuroscience Society, Poster  
Title: “Multimodal Signal Integration in the *Drosophila* CNS”
- 08/2012 23<sup>rd</sup> NeuroDoWo Marburg 2012, Presentation  
Title: “Integration of multimodal signals in the *Drosophila*  
central nervous system”



